INTERNATIONAL JOURNAL OF ENERGY STUDIES

e-ISSN: 2717-7513 (ONLINE); homepage: https://dergipark.org.tr/en/pub/ijes

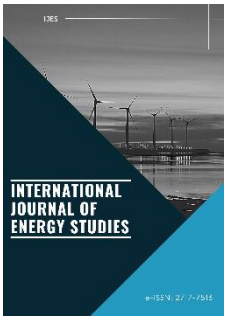

Research Article
Int J Energy Studies 2026; 11(1): 275-316
DOI: 10.58559/ijes.1829911

Received : 25 Nov 2025
Revised : 03 Feb 2026
Accepted : 11 Feb 2026

Numerical assessment of thermohydraulic performance in pipes with different arrangements of delta winglet pairs via the GEKO turbulence model

Hüseyin Zahit Demirağ[a*], Atila Abir İğci[b], Necip Hazer[c]

[a] *Yozgat Bozok University, Mechanical Engineering Department, 66100, Yozgat, Türkiye, ORCID:0000-0001-7289-4021*

[b] *Yozgat Bozok University, Mechanical Engineering Department, 66100, Yozgat, Türkiye, ORCID: 0000-0001-9679-4623*

[c] *Yozgat Provincial Directorate of Environment, Urbanization and Climate Change, 66100, Yozgat, Türkiye, ORCID: 0009-0004-8825-2153*

*(*Corresponding Author:zahit.demirag@yobu.edu.tr)*

Highlights

- Reliability of the GEKO Turbulence Model Confirmed
- Vortex Strength Dominates in CFPA Approach
- NCFPA Provides More Significant TEF Enhancement

You can cite this article as: Demirağ HZ, İğci AA, Hazer N. Numerical assessment of thermohydraulic performance in pipes with different arrangements of delta winglet pairs via the GEKO turbulence model. Int J Energy Studies 2026; 11(1): 275-316.

ABSTRACT

This study systematically investigates the effect of varying the number (N) of Delta Winglet Pairs ($DWPs$) under both constant ($CFPA$) and non-constant ($NCFPA$) total frontal projection areas on the thermal–hydraulic performance of tubular heat exchangers. Prior to these investigations, a detailed evaluation of the $GEneralized\ K\text{-}Omega$ ($GEKO$) turbulence model is performed to ensure its reliability for the present study. The Nusselt number (Nu) and Darcy friction factor (f) of a tubular domain fitted with delta winglet (DW) type vortex generators (VGs) are numerically investigated within $Re = 5000 - 25000$. The mean absolute deviations of 4.80%, 1.85% and 4.99% are attained with respect to the $Nu_{Exp.}$, $f_{Exp.}$ and $TEF_{Exp.}$ respectively. The free parameters are adjusted to $C_{SEP} = 1.75$ and the corresponding C_{MIXCOR} ($GEKO - 1.75$). Besides that, the validation of smooth pipe is also carried out and yields an average absolute deviations of 5.42% and 0.85% in comparison to the Dittus-Boelter and Petukhov correlation equations, respectively, with optimized free parameters are set to $C_{NW} = -1.18 - 2, C_{NW-SUB} = 1.7 - 2.5, C_{SEP} = 1$. Based on the analysis carried out within the scope of the $NCFPA$ approach, Thermal Enhancement Factors (TEF) exceeds unity for most cases, with the highest values of 1.28, 1.26, 1.22, and 1.17 at $Re = 5000$ for $N = 3 - 6$, respectively, indicating the strong contribution of longitudinal vortices at lower Reynolds numbers. In the $CFPA$ approach, although friction increased notably for $N = 3S$, the heat transfer enhancement outweighs the friction penalty, yielding TEF of 1.18 at $Re = 5000$ and ≈ 1.00 at $Re = 25000$. Overall, the $NCFPA$ approach showed a more pronounced TEF enhancement compared to $CFPA$, confirming the strong influence of DWP number and arrangement on thermal performance.

Keywords: GEKO turbulence model, Vortex generator, Thermal enhancement factor, Numerical analysis

1. INTRODUCTION

In the field of thermal enhancement, the application of passive techniques is preferred to the utilization of active methods [1] due to number of factors including the absence of external power through the system boundary [2][3], lacking the necessity of the application of specialized equipment, being an economical in cost, an easy to implement and a reliable for long-term use [4]. Vortex generator is one of the prevailing passive techniques [5][6]. Two types of vortices, with rotation axes either perpendicular and parallel to the flow, are generated by integrating vortex generators or obstacles, in various geometric shapes and sizes, to the flow field. These vortices are referred to as transverse and longitudinal vortices, respectively [7][8]. Although transverse vortices can facilitate local mixing, disruption of the boundary layer, and enhancement of heat transfer in a particular region, longitudinal vortices causing a continuous breakdown of the thermal boundary layer. Therefore, there has been considerable research, including both experimental and numerical assessment, conducted into the employment of longitudinal vortex generators (*LVGs*) in the quest to enhance thermal performance [9][10]. However, *LVGs* are also generate transverse vortices at the leading and trailing edges, although the strength of these vortices is relatively low [11]. Because of that, it is of great importance to conduct numerical studies in order to gain a detailed understanding of the effects of these vortices of different structures, formed within turbulent flow field, in terms of thermal performance and flow dynamics. In addition to that the computational modeling is particularly essential in areas where it is challenging or impossible to measure the parameters of the flow. Turbulence models in this regard playing a vital role in modeling of complex flow characteristics. Although more advanced models, such as Large Eddy Simulation (*LES*) and Direct Numerical Simulation (*DNS*), are present [12], two-equation turbulence models based on *RANS*, which account for the time-averaged effects of turbulence on the flow, have been demonstrated to produce results that are sufficiently close to experimental results particularly in the analysis of turbulent flow volumes fitted with *VGs*.

In this regard, Wang et al. [13] carried out both numerical and experimental study to analyze the impact of a new arrangement of planar and perforated vortex generators (*VGs*) in a heated tube in terms of heat transfer and flow characteristics within the range of *Re*=6060-21210. They stated that tubes with the modified *VG* showed periodic fluctuations in the strength of the primary longitudinal vortices, resulting in lower pressure loss but decreased thermal performance. The highest *TEF* of 1.44 was achieved with perforated *VGs*, exhibiting a perforation index of 7.8% and a pitch ratio of 3.27. Furthermore, the researchers compared various turbulence models and

determined that the *SST* k−ω turbulence model yielded the most accurate results in accordance with the experimental data. Wang et al. [14] also proposed a new perforated delta winglet (*PDW*) design. Using this winglet design, the highest *TEF* value was stated to be calculated as 1.49 for $PR = 1, w = 6\,mm, h = 2\,mm$ and $Re = 9000$ conditions. They also emphasized that the *SST* k−ω turbulence model was employed in the numerical part of analyses. Liu et al. [15] implemented both experimental and numerical investigation to assess the thermo-hydraulic performance of a heated tube containing a rectangular winglet vortex generator (*RWVG*) at *Re*=5000-17000. Their findings indicated that the *RWVG* exhibited a markedly enhanced heat transfer capability in comparison to the plain tube. A numerical analysis of heat transfer and flow characteristics was conducted by performing the *SST* k−ω turbulence model. They reached the conclusion that the maximum *PEC* is 1.18 for the following parameters: $\beta = 30°$, H_2/D = 0.5 and *Re*=5000. In order to improve the thermal performance of tubular heat exchangers, Wu et al. [16] propose a *VG* with multiple *V*-winglets and holes. They show that a higher number of *VGs* improves heat transfer, but increases friction. They emphasized that this frictional loss is reduced by positioning the holes on the *VGs*. In the numerical section of their study, the comparison showed that the highest deviation between the numerical and experimental results was 6.6%, confirming that the *SST* k−ω turbulence model provided the most accurate predictions. They achieved an increase in the Nusselt number ranging from 130.57% to 156.42% and attained a maximum performance evaluation factor of 2.83 with n=8 and *L*=25mm. Sun et al. [17] conducted both numerical and experimental investigations to examine the influence of design parameters on the thermal-hydraulic performance of heat exchanger tubes within the range of *Re*=5500-20000. The design parameters of the investigation are defined as follows: the number of rectangular winglets, $N = 4, 6, 8$; the winglet height ratio, $HR = 0.05, 0.1, 0.2$; as well as the pitch ratio, $PR = 1.57, 3.14,$ and 4.71. Based on their findings, they stated that the highest thermal enhancement factor of 1.27 was reached. In the selection of the turbulence model, they stated that they compared five different turbulence models with experimental data and, as a result of this comparison, they obtained the lowest deviation rate with the utilization of the *SST* k−ω turbulence model. Sun et al. [18] also carried out another experimental and numerical analysis to present the thermal-hydraulic performance of *CWVG* in the range of *Re*=5896-20283. They stressed that the standard k−ε model was selected over the previously utilized *RNG* k−ε model due to its higher accuracy, with a maximum deviation of 4.8% in comparison to other turbulence models. Xu et al**.** [19] conducted a numerical analysis at *Re*=6000-33000 to investigate the effects of varying angle of attack ($\beta = 0°, 15°, 30°$ and $45°$) and blocking ratio ($B = 0.1, 0.2$ and 0.3) on the heat transfer and friction

factor of delta winglet-type *VGs* placed in a pipe under a constant heat flux. Furthermore, five distinct turbulence models were evaluated, with the *SST* k−ω turbulence model exhibiting the lowest deviation rate for the smooth pipe validation study. Consequently, the highest thermal performance enhancement (*TPE*) was observed under the parameters of $\beta = 30°$ and $B = 0.1$. Liang et al. [20] employed a three-dimensional computational model to conduct a numerical analysis of the thermal performance and flow characteristics of delta winglet-type vortex generators (*WVGs*) within a pipe, utilizing a constant heat flux boundary condition across a range of Reynolds numbers between 6000 and 27000. This analysis was conducted for a variety of attack angle (β), inclination angle (α) and winglet length (L). In their numerical study, the *SST* k−ω turbulence model was highlighted to be employed. The resulting *TEF* value of 1.08 was stated to be obtained under the parameters of $\beta = 30°$ and $\alpha = 0°$ at Re=6000. The objective of the study conducted by Promvonge et al. [21] was to investigate the impact of a discrete *V*-type winglet (*DW*), positioned in a tubular heat exchanger, within the range of *Re*=4200-25800. The study involved the examination of the impact of various parameters, including the relative winglet height (R_B) and pitch (R_P), as well as the influence of two distinct flow arrangements, namely V −up and V −down. It was also noted that the Realizable k−ε turbulence model was employed. They concluded that the highest TEF values of approximately 1.99 and 2.02 were obtained for V −up and V −down, respectively. Zhang et al. [22] conducted a numerical and experimental investigation to evaluate the thermal-hydraulic performance of rectangular winglet vortex generators (*RWVGs*) positioned in a circular pipe in two distinct configurations: parallel (*P-RWVGs*) and *V*-shaped (*V-RWVGs*) in the range of *Re*=6000-20000. Moreover, they assessed five turbulence models and determined that the *RNG* k−ε turbulence model yielded the most accurate results in comparison to the experimental data. The results obtained through numerical analysis indicate that *P-RWVGs* generate a single longitudinal vortex, while *V-RWVGs* result in the formation of multiple longitudinal vortices. M.S. and Fernandes [23] carried out numerical investigation to examine the heat transfer performance and friction factor characteristics of circular tube fitted with semi-elliptical vortex generators within the range of *Re*=8000-26000. The parameters they investigated in their computational work include the aspect ratio ($AR = 1 - 6$), attack angle ($\alpha = 45° - 90°$), and the longitudinal pitch ($P = 30\ mm - 90\ mm$). Furthermore, they employed the *RNG* k−ε turbulence with *EWT* for the analysis of the turbulent computational domain. They concluded that the overall *TEF* ranged from 0.86 to 1.19 and exhibited a declining trend with an increase in aspect ratios and attack angles. Min et al. [24] conducted a computational analysis to increase thermal performance of tubular heat exchanger by integrating twisted belts

and delta wing vortex generators (*DWVG*) combination in a circular tube. They selected the Standard k−ω turbulence model for the computational analysis carried out within the range of *Re*=5000-25000. The effects of twist ratio (y/w), attack angle (α), pitch (P), and vortex generator configuration were investigated, and it was determined that the optimal configuration is a staggered when the belt is twisted in a counter-clockwise direction. Employing both numerical and experimental techniques, Jayranaiwachira et al. [25] examined the heat transfer and flow characteristics of a tubular heat exchanger with louver-punched triangular baffles (*LPTBs*) at *Re*=4760-29270. They applied the Realizable k−ε turbulence model in numerical studies in order to visually reveal the thermal and flow behaviors in the pipe along with the validation of the selected experimental data. They stated that the numerical results were determined to exhibit a high degree of consistency with the experimental data. Habchi et al. [26] investigated the potential for enhancing heat transfer in a circular pipe using vortex generators (*VGs*) and protrusions through the numerical investigation undertaken at Re=7500-15000. A total of twelve configurations of trapezoidal *VGs* were subjected to an in-depth analysis with the objective of evaluating their performance in terms of heat transfer and pressure drop under turbulent flow conditions. For the purpose of achieving this objective, they employed the *RNG* k−ε turbulence model. They emphasized the fact that the *RNG* k−ε turbulence model provides a significant advancement over the Standard k−ε model by incorporating the effects of strong streamline curvature, vortices, and swirl, resulting in a more accurate solution.

Upon reviewing the literature, the motivation for this study arises from the observation that, although *DWPs* have been extensively utilized to initiate the formation of longitudinal vortices (*LVs*) to enhance convective heat transfer in thermal systems, the majority of previous research has primarily focused on geometric optimization, arrangement patterns, and angle of attack. However, the influence of the number of *DWPs* on the overall thermohydraulic performance has received limited attention at tubular heat exchangers. In particular, no study has been identified that systematically investigates the effect of varying the number (*N*) of *DWPs* while maintaining a constant total frontal projection area (*CFPA*) and aspect ratio (*AR*) in tubular heat exchangers. This aspect is crucial because isolating the influence of the VG number under constant geometric constraints enables a more direct understanding of the relationship between flow structure and heat transfer enhancement. In this regard, a comprehensive analysis has been conducted to evaluate the effect of varying the number of *DWPs* under both constant (*CFPA*) and non-constant (*NCFPA*) total frontal projection areas on the thermal–hydraulic performance of tubular heat exchangers.

Addressing this gap is essential for developing a more complete understanding of how the number and the resulting arrangement of *VGs* affect both heat transfer augmentation and flow resistance characteristics.

In addition, the application of the recently developed *GEKO* turbulence model adds a distinctive value to this study. A review of the literature shows that the widely adopted *RANS*-based two-equation turbulence models for numerical analysis of *VG*-induced turbulent flows are predominantly either k$-\varepsilon$ or k$-\omega$ based. However, detailed investigations on the application of the k$-\omega$ based *GEKO* model to the thermo-hydraulic performance of flows with *VGs* are limited. The predictive performance of turbulence models is highly dependent on the flow structures to which they are applied, including free shear, wall-bounded, separated, swirling, and transitional flows. Therefore, to establish the reliability of the *GEKO* turbulence model under such complex flow conditions, it is essential to conduct a systematic performance assessment and to compare the computational results with available experimental data. Accordingly, the performance of the *GEKO* turbulence model is evaluated, with the framework focusing on the validation of key flow metrics, specifically the Nusselt number and Darcy friction factor, across a range of Reynolds numbers. In order to fulfill this aim the verification analysis are carried out for both turbulent flow volume with/without *VG*s. In this respect, the experimental Nusselt number and Darcy friction factors at different Reynolds numbers in a circular cross-sectional turbulent flow volume with *DWs*, which is considered to contain the above mentioned complex flow features, are verified. In addition to that smooth pipe Nu_0 and f_0 values are also verified with established Dittus-Boelter and Petukhov correlation equations in the range of $Re = 5000 - 25000$, respectively.

2. COMPUTATIONAL MODEL AND METHODOLOGY

In the following section, the computational framework applied in this numerical study is introduced in detail, encompassing the computational domain configuration, selected turbulence model, numerical formulations, and the procedure adopted for the mesh independence test.

2.1. Computational Model Specifications

In this study, the effects of positioning of different numbers of *DWPs* in a single row in terms of thermo-hydraulic performance are investigated within the range of $Re = 5000 - 25000$. This section is analyzed in two parts. Initially, the number of *DWPs* in a single row without any change in their geometrical dimensions (*NCFPA*), is arranged as $N = 6, 5, 4$ and 3, respectively.

The geometric configurations and details of computational fluid domains for a pipe equipped with different number of *DWPs* are shown in Figure 1. The computational fluid domain of the circular pipe equipped with *DWPs* consists of three main sections: the inlet, test, and exit regions, respectively. Additionally, the Figure 1 also provides the information about the size of the computational fluid domain of test region fitted with different number *DWPs* in a single row. Considering symmetry boundary conditions, fractions of the total flow domain, $1/12$, $1/10$, $1/8$, and $1/6$, are utilized as the computational domain for cases with $N = 6, 5, 4$ and 3, respectively.

The following part of numerical investigation differs from the initial part in that it examines the impact of varying numbers of *DWPs* on heat transfer and friction factors, while ensuring consistency in the total frontal projection areas ($\sum A_{\text{Projection,N=6}} = \sum A_{\text{Projection,N=3S}}$). Additionally, the aspect ratio (*AR*=The ratio of the height to length of *DWP*, $AR_{DWP} = h/l = 2$) of DWPs remain unchanged for scenarios with $N = 6$ and $N = 3S$, as the aspect ratio is identified as a critical parameter in *VG* geometry [27][28]. Accordingly, in order to maintain the aspect ratio while keeping the total frontal projection area equal to the $N = 6$ case, the *DWP* is scaled up to $S \cong 1.46{:}\,1$ (defined as $N = 3S$) when the number of *DWPs* in a single row is 3. In this context, Figure 2 illustrates the configuration of *DWPs* with two distinct numbers, $N = 6$ [$S = 1{:}\,1$], $N = 3S$ [$S = 1.46{:}\,1$], and $N = 3$ [$S = 1{:}\,1$], in a common-flow-up (*CFU*) configuration. Notably, in both initial and following parts of the computational work, *DWP*s with $N = 6$ configuration is utilized as the reference.

In order to ensure that the flow is hydrodynamically fully developed at the inlet of the test section, the length of the inlet region should be at least ten times the hydraulic diameter of the pipe [$D_h = 0.052\,m$][29]. Hence, the length of the inlet zone is chosen as $L_{Inlet} = 0.8\,m$ [$\approx 15D_h$]. Furthermore, the length of the exit region is assigned as $L_{Exit} = 0.4\,m$. In conclusion, the test region length is also set to $L_{Test} = 0.5\,m$. The entrance of the test section in the flow domain exhibits a markedly higher heat transfer coefficient. Thus, the positioning of DWPs at a relative distance from the starting point of test section is important to achieve higher thermal performance along test region. Henceforth, *DWPs* with an angle of attack of $\theta = 30°$ are situated at distance of $50\,mm$ from the starting point of flow domain test region in *CFU* configuration in order to initiate *LVs* along the test region to disrupt the growth of thermal boundary layer and thereby augment heat transfer reasonably.

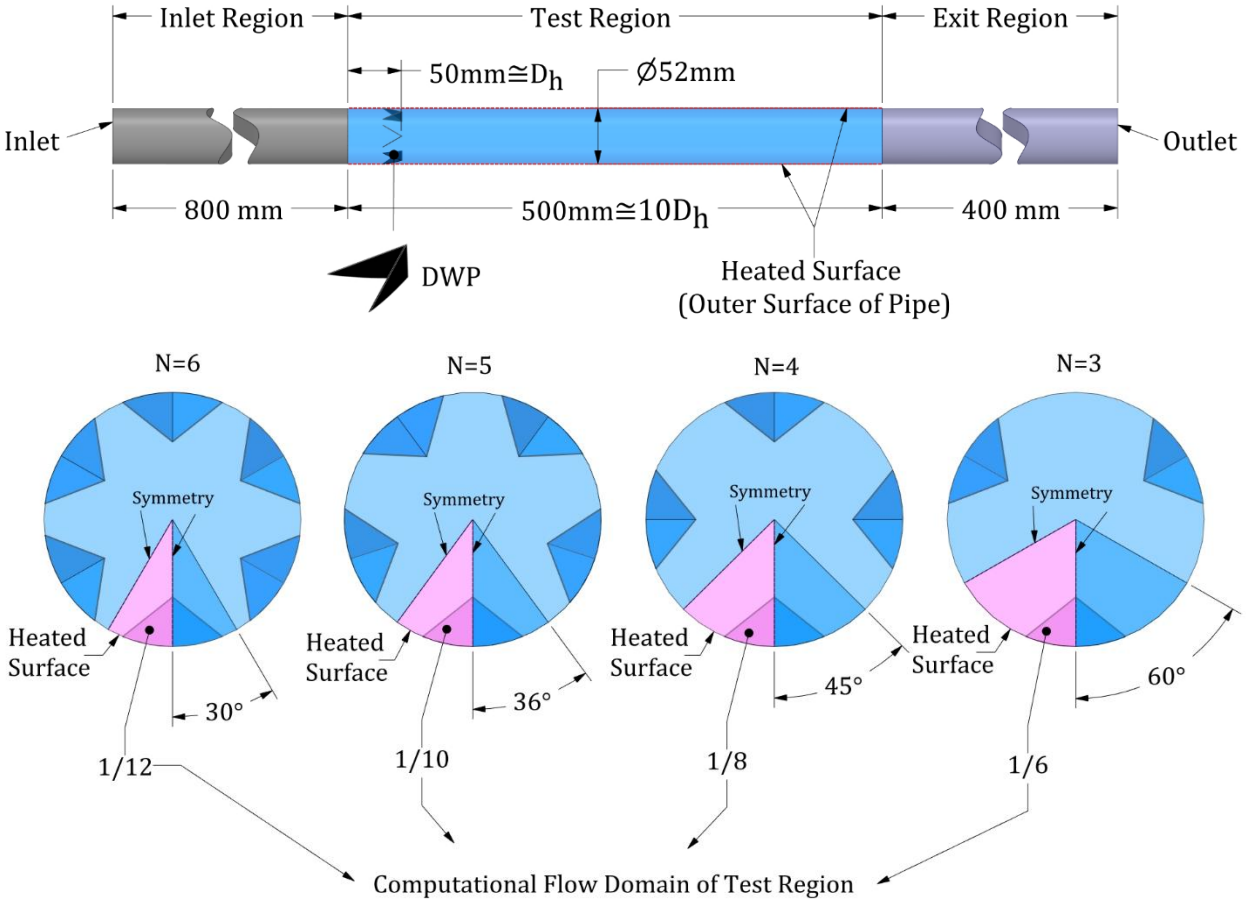

Figure 1. Geometric configuration of computational flow domain of pipe fitted with *DWPs* at N=6, 5, 4, 3

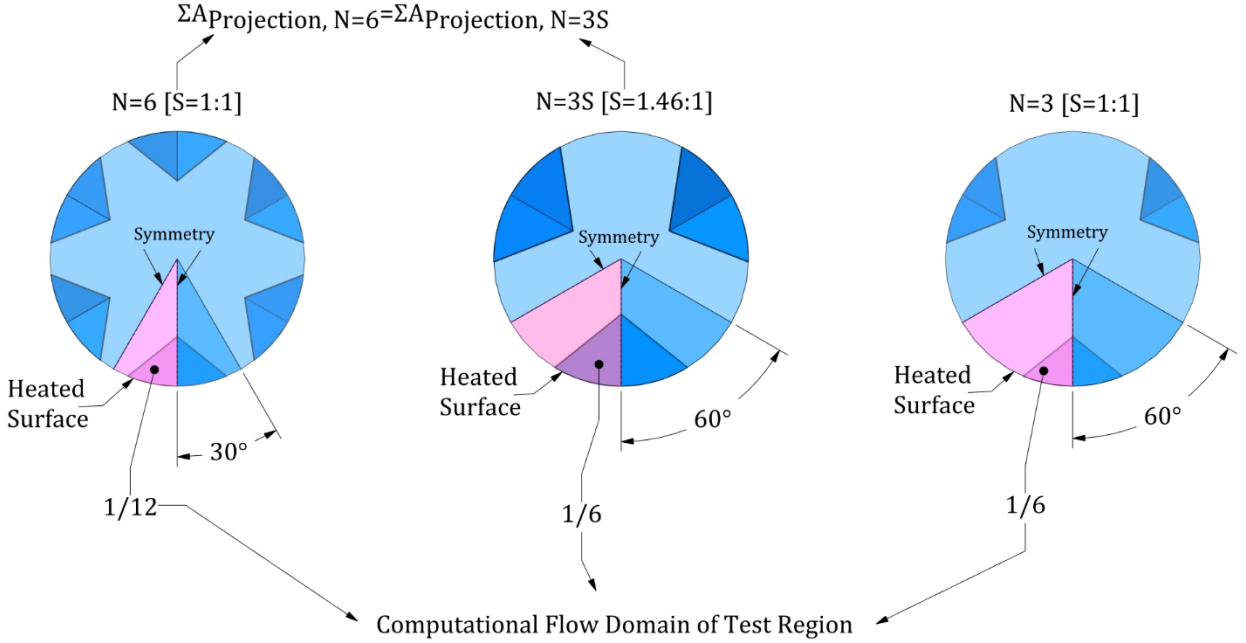

Figure 2. Configuration of *DWPs* on test region for cases of N=6 [S=1:1], N=3S [S≅1.46:1] and N=3 [S=1:1]

The geometric specifications of the *DWP* utilized in this computational analysis are also provided in Figure 3. The height and base length values of the *DWP* are $h = 10\,mm$ and $l = 20\,mm$, respectively. The DWP is mounted on the curved pipe surface; therefore, the planar projection length of its base is taken as the reference for defining the base length.

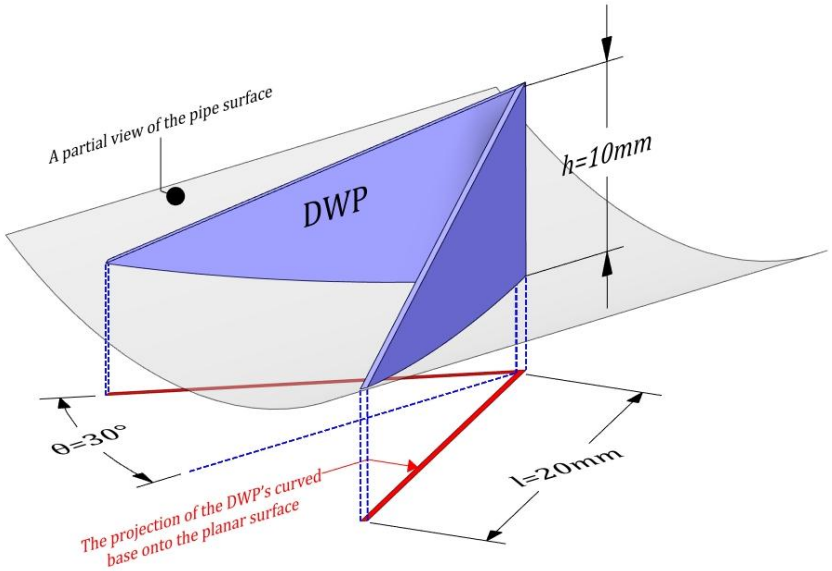

Figure 3. Geometric details of *DWP* [θ=30°]

It should be noted that the experimental validation study for *DW* [30] served as a reference for determining both the pipe diameter [$D_h = 0.052\,m$], the inlet and exit regions of the computational domain, and the geometry of the vortex generator (*DWP*). In addition, in the experimental study selected for numerical validation [30], *DWs* are arranged in two rows along a test section with a length of $1000\,mm$. Accordingly, since all parametric cases in the present study employ a single-row arrangement of *VGs*, the test section length is set to $L_{Test} = 0.5\,m$, as previously noted. Furthermore, given the similarity between the experimental flow conditions ($\alpha = 40°$, $s = 10\,mm$ and $h = 10mm$) and the present numerical study, the free parameters, selected during the experimental validation of *DW* ($\alpha = 40°$, $s = 10\,mm$ and $h = 10mm$) are set to $C_{SEP} = 1.75$, in contrast to the smooth pipe verification study of (Nu_0 and f_0). Consequently, the performance of the $GEKO - 1.75$ turbulence model under experimental flow conditions is assessed, confirming its suitability for the subsequent analyses.

2.2. Numerical Data Analysis

The non-dimensional numbers, presented below, are employed in the computational assessment of both the smooth pipe and the pipe equipped with a *DWPs*.

- Nusselt Number [Nu] [29]

$$Nu = \frac{h\,D_h}{k_f} = \frac{q''\,D_h}{k_f[T_w - T_b]} \tag{1}$$

The variables are defined as follows: T_b, T_w, q'', k_f, D_h, and h are refer to the volume-weighted average of fluid temperature on test region, the area-weighted average of heated surface temperature, heat flux employed on heated surface, thermal conductivity of fluid, hydraulic diameter of pipe and convective heat transfer coefficient, respectively.

- Reynolds Number [Re] [29]

$$Re = \frac{\rho V_m D_h}{\mu} \tag{2}$$

where, ρ represents the density of fluid, V_{m} denotes the volume-weighted averaged velocity of the fluid on test region and μ refers to the dynamic viscosity of fluid.

- Darcy Friction Factor [f] [29]

$$f = \frac{\Delta P}{\left(\frac{L}{D_h}\right)\left(\frac{\rho {V_m}^2}{2}\right)} \tag{3}$$

where ΔP represents the pressure difference along test region and L denotes the distance between the selected planes that fully encompass the fluid domain of the test section. Area-weighted average pressure values are obtained at these planes.

- Thermal Enhancement Factor [TEF] [31][32]

$$TEF = \left[\frac{Nu}{Nu_0}\right]\left[\frac{f}{f_0}\right]^{-1/3} \tag{4}$$

where, the subscript "0" represents the smooth pipe.

2.3. Governing Equations

A well-established understanding is that turbulent flows, characterized by their eddy motion, exhibit notable fluctuations in variable such as velocity, temperature, and pressure despite being in a steady-state conditions. However, focusing on the analysis of time-averaged flow characteristics, such as average velocity, pressure and stresses, provides sufficient information

about their overall effect on flow behavior. Reynolds decomposition is employed to decompose turbulent motion into average and fluctuating components, yielding a time-averaged continuity, momentum (Reynolds-Averaged Navier-Stokes - *RANS*), and energy equations. In this regard, to examine the incompressible turbulent airflow in a circular pipe with a hydraulic diameter of $D_{\mathrm{h}} = 0.052\ m$, the *RANS* equations are applied. The time-averaged equations can be presented in tensor notation, provided that the fluid properties are considered constant, the flow is steady and incompressible, and body forces and viscous dissipation are not taken into account. Under these assumptions, the governing equations can be expressed as follows [33]:

- Continuity equation

$$\frac{\partial}{\partial x_i}(\rho u_i) = 0 \tag{5}$$

- Momentum equation

$$\frac{\partial}{\partial x_j}\left(\rho u_i u_j\right) = -\frac{\partial p}{\partial x_i} + \frac{\partial}{\partial x_j}\left[\mu\left(\frac{\partial u_i}{\partial x_j} + \frac{\partial u_j}{\partial x_i}\right) - \overline{\rho {u_i}' {u_j}'}\right] \tag{6}$$

- Energy equation

$$\frac{\partial}{\partial x_i}[\rho u_i T] = \frac{\partial}{\partial x_i}\left[\Gamma \frac{\partial T}{\partial x_i} - \overline{\rho {u_i}' T'}\right] \tag{7}$$

In order to calculate Reynolds stresses, the Boussinesq approach, based on average velocity gradient, is employed and further details regarding the Boussinesq approach is detailed as follows.

$$-\rho\overline{u_i' u_j'} = \mu_t\left(\frac{\partial u_i}{\partial x_j} + \frac{\partial u_j}{\partial x_i}\right) - \frac{2}{3}\left(\rho k - \mu_t \frac{\partial u_i}{\partial x_i}\right)\delta_{ij} \quad \text{and} \quad -\rho\overline{u_i' T'} = \Gamma_t \frac{\partial T}{\partial x_i} \tag{8}$$

The variable of k denotes as the turbulent kinetic energy and formulated as $k = \overline{u_i' u_i'}/2$, while the variable of δ_{ij} is defined as the Kronecker delta function. The terms Γ and Γ_t represent molecular heat conduction coefficient and turbulent heat conduction coefficients, respectively and these terms are formulated as follows.

$$\Gamma = \frac{\mu}{Pr} \quad \text{and} \quad \Gamma_t = \frac{\mu_t}{Pr_t} \tag{9}$$

The variable of μ_t denotes the eddy viscosity, indicating the momentum transported by turbulent eddies. Contrary to the molecular viscosity, μ_t presents different values in various flow conditions and thus an accurate evaluation of this variable requires the implementation of a proper turbulence model.

2.4. Boundary Conditions

In the present computational study, a three-dimensional flow is implemented in steady-state regime and the fluid flow (air) is considered incompressible, turbulent and ignores viscous dissipation, body forces and radiative heat transfer. The symmetry boundary conditions as shown in Figure 1 and Figure 2 are taken into account in numerical calculations. The no-slip boundary condition is applied at the fluid-solid interfaces, including the inner pipe wall and the surfaces of the *VGs*, despite the solid components themselves (pipe thickness and the vortex generators) are not being modeled in computational domain. Furthermore, the assumption is that all surfaces are perfectly smooth and impermeable. A constant heat flux boundary condition is imposed on the outer wall of the pipe at computational domain test region, which is identified as the heated surface [$q'' = 600\ W/m^2$], as shown in Figure 1, Figure 2 and

Figure **4**. Heat losses through the pipe walls are neglected. In addition, an adiabatic wall boundary condition is implemented for contact surfaces between the fluid and the walls of *DWPs*. At the pipe inlet, a uniform air velocity profile is established [$U_r = U_\theta = 0$ and $U_z = V_{in}$)], and the outlet is subject to a zero gauge pressure condition [$P_{out} = 0$] . The fluid temperature is set to $T_{in} = 293.15$ K, at the inlet section. The thermophysical properties of air are accounted for at the bulk temperature [T_b].

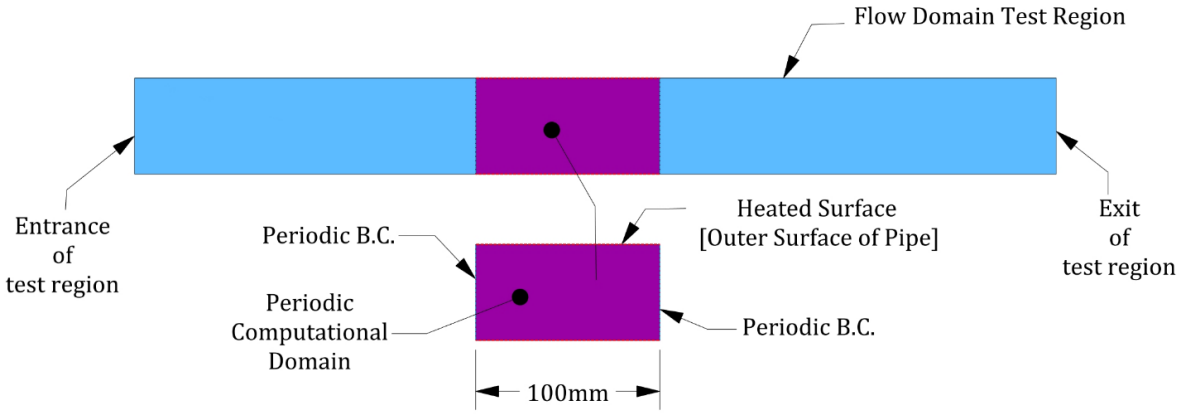

Figure 4. Computational domain of the smooth pipe, including the geometric configuration and imposed boundary conditions

Under fully developed flow conditions in a smooth pipe, the flow and heat transfer characteristics along the entire pipe or test section can be determined without explicitly accounting for the entrance region by employing a periodic solution domain. Accordingly, periodically fully developed turbulent flow and heat transfer solution method is applied for the smooth pipe computations in this study. Schematic representations and boundary conditions of the computational fluid domain for the smooth pipe is detailed in

Figure **4**. This approach is taken due to the implementation of periodic boundary conditions, aiming to optimize computational resources and time, alongside ensuring fully developed flow conditions.

2.5. Numerical Method

Numerical computations are performed using *ANSYS* Fluent Computational Fluid Dynamics [*CFD*] software. The governing equations are discretized using the finite volume method. The pressure-velocity coupling is handled by a robust coupled algorithm, with a second-order upwind scheme used to discretize the convective terms. Convergence is achieved when the residuals for all equations are less than 10^{-4}, except for the energy equation, which is less than 10^{-7}. Although residuals are used to assess convergence, the volume-weighted average temperature of the test region in the fluid domain, which remains unchanged from iteration to iteration, is also taken into account in the convergence criteria.

2.6. Turbulence Model

In order to analyze internal turbulent flows with *VGs* under steady state conditions, the utilization of an appropriate turbulence model in the application of the *RANS* equations is of great importance. In this computational research, the numerical analysis of turbulent flows is carried out using the *GEKO* turbulence model, which is based on the k$-\omega$ formulation recently developed by *ANSYS*. The turbulence model used in this study is the *GEKO* turbulence model, and the general formulation of this model is given below, as it is expressed by Menter et al. [34].

$$\frac{\partial(\rho k)}{\partial t}+\frac{\partial\left(\rho u_j k\right)}{\partial x_j}=P_k-C_\mu\rho k\omega+\frac{\partial}{\partial x_j}\left[\left(\mu+\frac{\mu_t}{\sigma_k}\right)\frac{\partial k}{\partial x_j}\right] \quad (10)$$

$$\frac{\partial(\rho\omega)}{\partial t}+\frac{\partial\left(\rho u_j\omega\right)}{\partial x_j}=C_{\omega1}F_1\frac{\omega}{k}P_k-C_{\omega2}F_2\rho\omega^2+\rho F_3CD+\frac{\partial}{\partial x_j}\left[\left(\mu+\frac{\mu_t}{\sigma_\omega}\right)\frac{\partial\omega}{\partial x_j}\right] \quad (11)$$

$$\mu_t=\rho\nu_t=\rho\frac{k}{\max(\omega,S/C_{REAL})};\ C_{REAL}=\frac{1}{\sqrt{3}}\approx0.577 \quad (12)$$

$$P_k=-\tau_{ij}\frac{\partial u_i}{\partial x_j} \quad (13)$$

$$\tau_{ij}^{EV}=-\rho\overline{u_i'u_j'}=\mu_t2S_{ij}-\frac{2}{3}\rho k\delta_{ij} \quad (14)$$

$$CD=\frac{2}{\sigma_\omega}\frac{1}{\omega}\frac{\partial k}{\partial x_j}\frac{\partial\omega}{\partial x_j} \quad (15)$$

$$\tau_{ij}=\tau_{ij}^{EV}-C_{CORNER}\frac{1.2\mu_t}{\max\left(0.3\omega,\sqrt{0.5(S^2+\Omega^2)}\right)}\left(S_{ik}\Omega_{kj}-\Omega_{ik}S_{kj}\right) \quad (16)$$

$$S_{ij}=\frac{1}{2}\left(\frac{\partial u_i}{\partial x_j}+\frac{\partial u_j}{\partial x_i}\right) \quad (17)$$

$$\Omega_{ij}=\frac{1}{2}\left(\frac{\partial u_i}{\partial x_j}-\frac{\partial u_j}{\partial x_i}\right) \quad (18)$$

$$S=\sqrt{2S_{ij}S_{ij}} \quad (19)$$

$$\Omega=\sqrt{\Omega_{ij}\Omega_{ij}} \quad (20)$$

In order to achieve different objectives in a wide range of flow scenarios, the free parameters of the *GEKO* turbulence model are implemented by user-adjustable functions, including F1, F2 and F3. F1, F2 and F3 are only available within the *ANSYS* Fluent *CFD* software package and are not publicly available in the open literature. To ensure compatibility with experimental data, the results obtained with the *GEKO* turbulence model contain six free parameters. The ranges of these parameters and their default values are shown in Table 1 below.

Table 1. Ranges and default values of free parameters of the *GEKO* Turbulence Model [34].

Free Coef.	Range	Default	Function

C_{SEP}	[0.7 – 2.5]	1.75	Tuning prediction of flow separation, affects the overall flow dynamics
C_{NW}	[-2.0 – 2.0]	0.5	Affect the dynamics of wall shear stress and heat transfer
C_{MIX}	[… 0.5 – 1.0 …]	C_{MixCor}	Affects the flow mixing that occurs due to free shear flows (*)
C_{JET}	[0.0 – 1.0]	0.9	Alters the rate of spreading in jet flows
C_{CORNER}	[0.0 – 1.5]	0.0 or 1.0	Affects secondary flows in corners but is deactivated by default (C_{CORNER} = 0)
C_{CURV}	[0.0 – 1.5]	0.0 or 1.0	Affects the impact of streamline curvature in the flow, but is deactivated by default (C_{CURV} = 0)

(*) The recommended range for the C_{MIX} parameter is a guide only and the actual value may vary depending on the accuracy of experimental measurements. The C_{MIX} parameter is set by default to ensure that changes in C_{SEP} do not adversely affect the free mixed layers and is calculated using a formula based on C_{SEP} ($C_{MixCor} = 0.35 sign(C_{SEP} - 1)\sqrt{(|C_{SEP} - 1|)}$). However, where flow mixing is severe, users may use values other than those recommended to match experimental results. C_{NW_SUB} which has a default value of 1.7 and affects the wall shear stress, is another specific parameter in the GEKO turbulence model. [34].

2.7. Grid Structure of Smooth Pipe and Pipe Fitted with DWPs

Mesh independence tests are performed for both the smooth pipe and the reference case of pipe fitted with *DWPs* at $N = 6$ to obtain an accurate computational solution using an optimal number of cells that ensures the conservation of computational resources. In accordance with the preceding methodology, the smooth pipe mesh independence test is initially conducted at $Re = 25000$ for four distinct cell numbers, and the resulting Nu_0 and f_0 values are presented in Figure 5.

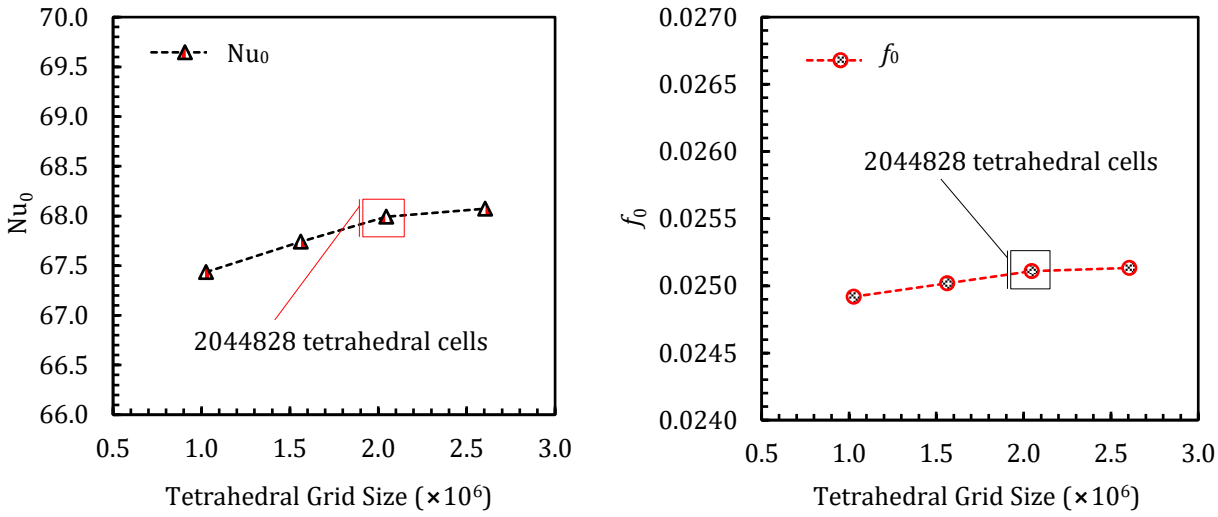

Figure 5. Mesh independence test of smooth pipe [35]

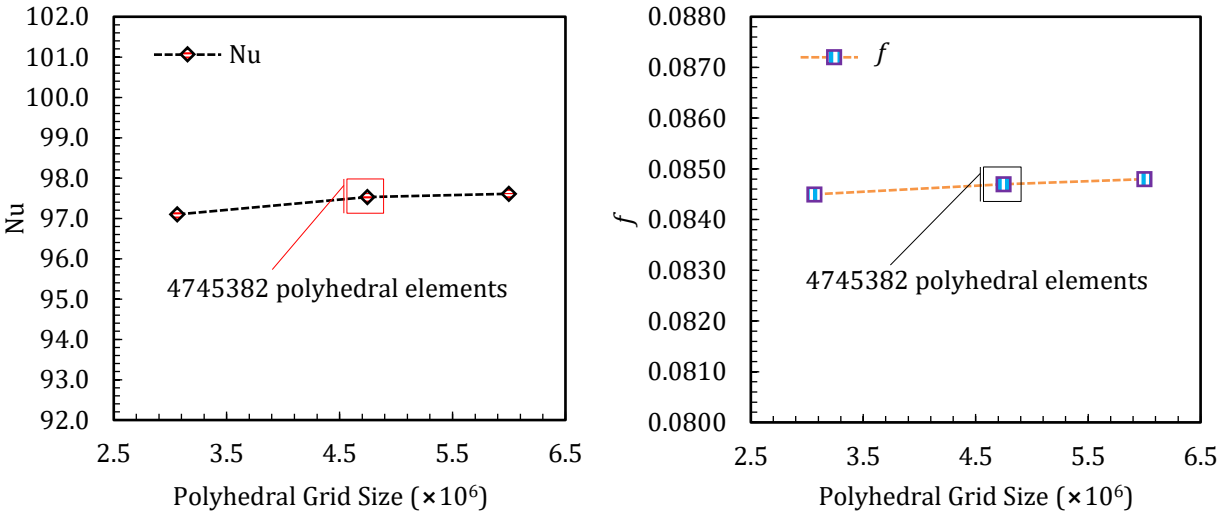

Figure 6. Mesh independence test of pipe fitted with *DWPs* at N=6

In the subsequent stage of the investigation, the mesh structure with three different polyhedral grid sizes are analyzed at $Re = 25000$ for the reference case of *DWPs* at $N = 6$. The resulting *Nu* and *f* values are presented in Figure 6 in a comparative manner. The computational results indicate that exceeding the number of cells beyond the tetrahedral cell number of $\approx 2.04 \times 10^6$ and the polyhedral cell number of $\approx 4.75 \times 10^6$ for the purpose of attaining an accurate numerical solution for smooth pipe and pipe inserted with *DWPs* at $N = 6$ are not necessary as presented in Figure 5 and Figure 6, respectively.

In both cases of the smooth pipe as well as the pipe equipped with *DWPs*, the computational domain are structured in such a way that the mesh grids are divided into distinct sections. Upon examining the smooth pipe, computational domain given in Figure 7 consists of central region and

the enclosing the edge regions, adjacent to the heated surface, features finer mesh grids compared to the central region. Furthermore, the number of elements on the heated surface is further increased. The aim is therefore to ensure accurate calculations of velocity and temperature gradients in these regions.

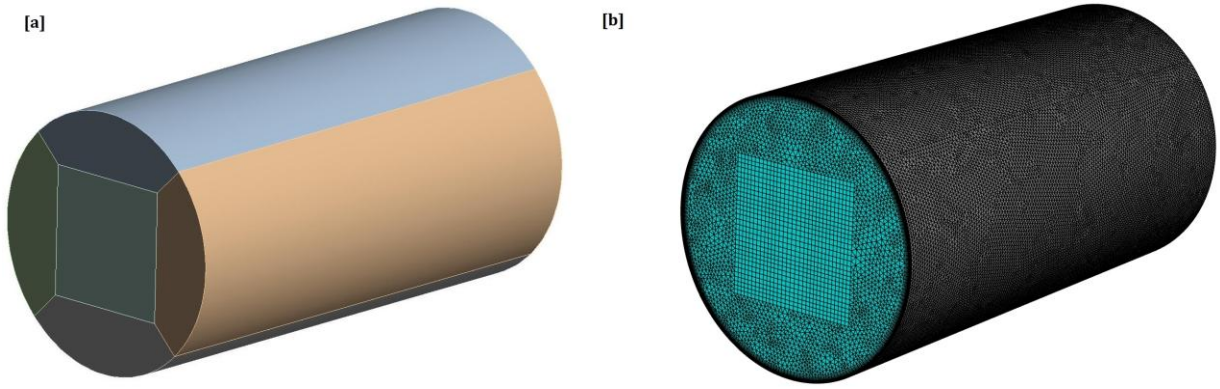

Figure 7. Smooth pipe: (a) flow domain and (b) grid structure consisting of 2044828 tetrahedral elements [35]

Upon analysis of the pipe with *DWPs*, a similar approach has been applied to the computational domain and resulting the computational test region composed of multiple sections besides inlet and exit regions. The number of polyhedral cells are considerably higher compared to other computational domains, including inlet and exit regions. Further examining of the mesh grid bounded by the dashed line reveals that the section containing the *DWP* has the densest mesh grid within the computational domain test region (Figure 8). This is because it is vital to accurately compute velocity and temperature gradients, particularly with the presence of the strongest vortices occurring right after the *VG* (trailing end of *DWP*).

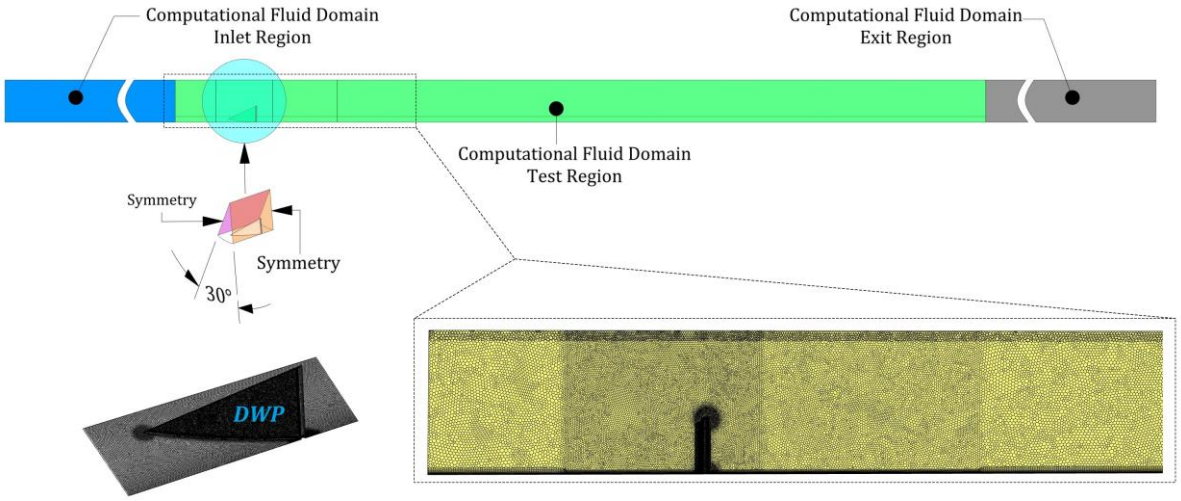

Figure 8. Pipe fitted with *DWPs* [N=6 and θ=30°]: grid structure consisting of 4745382 polyhedral elements

The presence of strong vortices leads to suppression of the growth of thermal boundary layer on heated surface. Thus, the thinnest first cell height $[0.025mm]$ in the inflation layer is chosen at the section encapsulating *DWP*. As vortices lose their strength along the flow direction due to viscous forces, it is observed that the number of polyhedral elements decreases in subsequent sections following the section containing *DWPs*, and correspondingly, the first cell height increases from $0.025mm$ to $0.04mm$ and is eventually set to $0.05mm$ at other parts of computational domain in compliance with the dimensionless wall distance of $y^+ \leq 1$ [36]. Moreover, at least ten inflation layers have been identified for both cases smooth pipe and the pipe equipped with *DWPs*. Finally, the selected growth rate is 1.15.

3. RESULTS AND DISCUSSION

This section evaluates the impact of varying the number of *DWPs* under constant (*CFPA*) and non-constant (*NCFPA*) frontal projection areas on the thermal–hydraulic performance, and presents a comprehensive numerical validation confirming the capability of the *GEKO* turbulence model in accurately predicting turbulent internal flows both in the presence and absence of *VGs*.

3.1. The Performance of GEKO Turbulence Model: DW inserted Pipe

This part of numerical work, concerning the validation of the pipe fitted with DWs at $\alpha = 40°$, $s = 10\ mm$, and $h = 10\ mm$, is derived from the master thesis, entitled "Numerical Investigation of the Thermal Performance of Innovative Vortex Generator Designs Placed on the Heated Surface in a Pipe with the GEKO Turbulence Model" [35].The selected experimental data for turbulent

flow through a pipe equipped with DWs at an attack angle of $\alpha = 40°$, a spacing of $s = 10$ mm between the leading edges, and a height of $h = 10\ mm$ [30], are numerically validated in terms of Nu and f over the Reynolds number range of $5000 - 25\ 000$ using the GEKO turbulence model. The GEKO turbulence model manual states that C_{SEP} is identified as the primary free parameter for model calibration.

While the GEKO turbulence model provides additional tunable parameters, it is highlighted that the default value of $C_{SEP} = 1.75$ replicates the behavior of the SST k$-\omega$ turbulence model [34]. Previous studies have demonstrated that the SST k$-\omega$ model performs exceptionally well in predicting turbulent internal flows featuring VGs. Therefore, in the present study, the GEKO turbulence model with $C_{SEP} = 1.75$ is employed for the numerical validation of the experimental data. Under the DW configuration with $\alpha = 40°, s = 10\ mm, h = 10\ mm$ and $PR = 9.61$, a numerical validation study is performed against the corresponding experimental measurements, with the resultant data presented in Figure 9 and Figure 10. When employing the $GEKO - 1.75$, the average absolute deviations from the experimental data are calculated to be 4.80% for Nu and 1.85% for f. Furthermore, following the determination of Nu_0 and f_0 values over the Reynolds number range of $5000 - 25000$, The comparison between the numerical and experimental TEF results is also presented in Figure 11. The results indicate an average absolute deviation of 4.99%. These deviation levels fall well within the acceptable margins reported in the literature [18][37]. Accordingly, the $GEKO - 1.75$ model is adopted in all following parametric analyses. It is also noteworthy that, in the present study, the default values of free parameters of the GEKO turbulence model is applied globally throughout the computational domain rather than zonally.

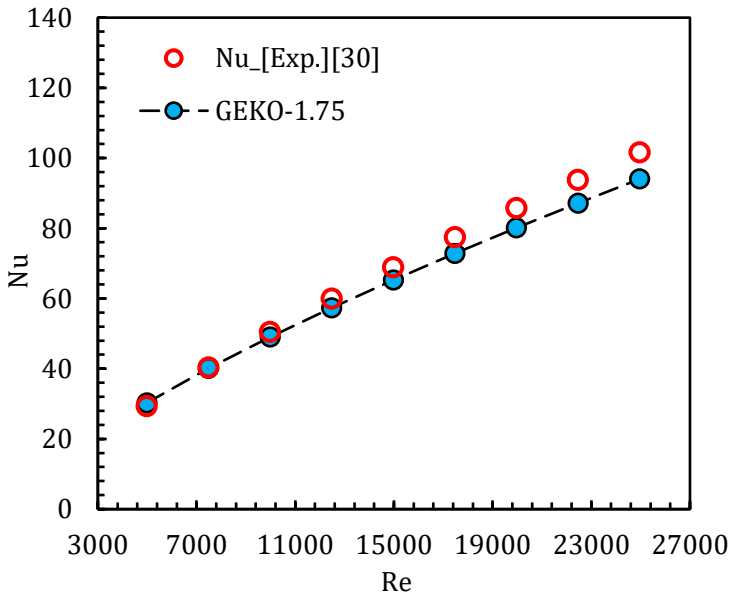

Figure 9. Change of *Nu* values relative to Reynolds number for *DWs* at α=40°, s=10 mm, h=10 mm and PR=9.61

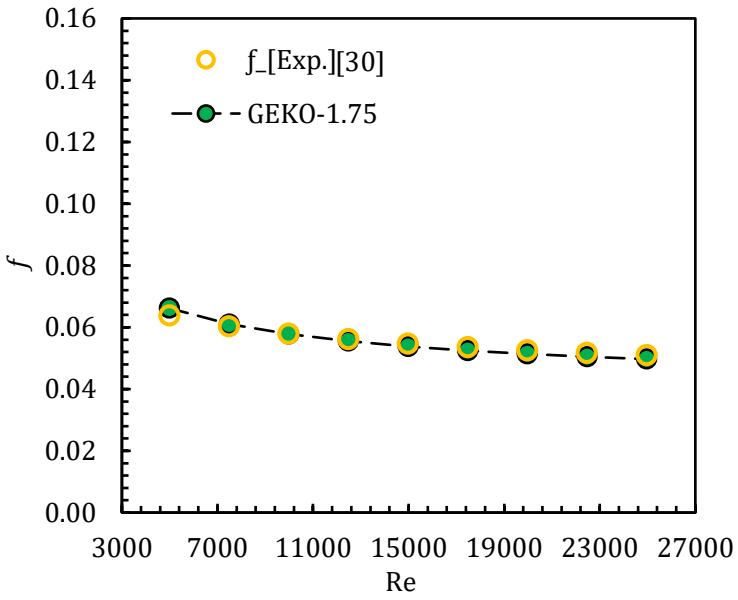

Figure 10. Change of *f* values relative to Reynolds number for *DWs* at α=40°, s=10 mm, h=10 mm and PR=9.61

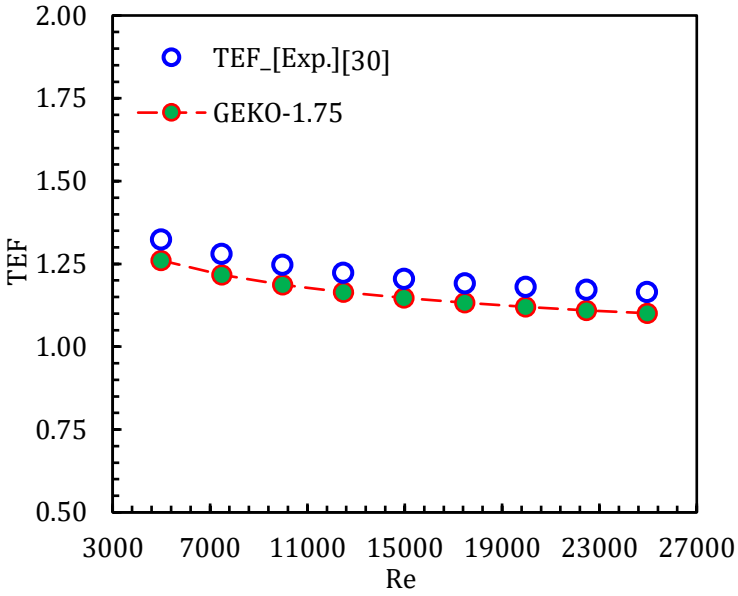

Figure 11. Change in TEF values relative to Reynolds number for *DWs* at α=40°, s=10 mm, h=10 mm and PR=9.61

3.2. The Performance of GEKO Turbulence Model: Smooth Pipe

This part of computational assessment concerning the validation of the smooth pipe is derived from the master thesis, entitled "*Numerical Investigation of the Thermal Performance of Innovative Vortex Generator Designs Placed on the Heated Surface in a Pipe with the GEKO*

Turbulence Model" [35]. In order to demonstrate the performance of *GEKO* turbulence model in predicting turbulent flow and validate the precision of the numerical simulation, the smooth pipe Nusselt number [Nu_0] and Darcy friction factor [f_0] values, are compared with Dittus-Boelter and Petukhov correlation equations, respectively within the range of $Re = 5000 - 25000$. The correlation equations of Dittus-Boelter and Petukhov are expressed as follows:

- Dittus-Boelter [38]

$$Nu = 0.023\ Re^{0.8} Pr^{0.4} \tag{12}$$

- Petukhov [39]

$$f = [0.79\ ln(Re) - 1.64]^{-2} \tag{13}$$

The resultant data attained by the numerical assessment for the case of smooth pipe in terms of Nu_0 and f_0 values are presented with the values obtained from the Dittus–Boelter and Petukhov correlation equations in Figure 12 and Figure 13 respectively, in comparative manner. Upon examination of the data, the mean absolute deviation rates for the values of Nu_0 and f_0 are calculated to be 5.42% and 0.85% in comparison to the Dittus-Boelter and Petukhov correlation equations, respectively.

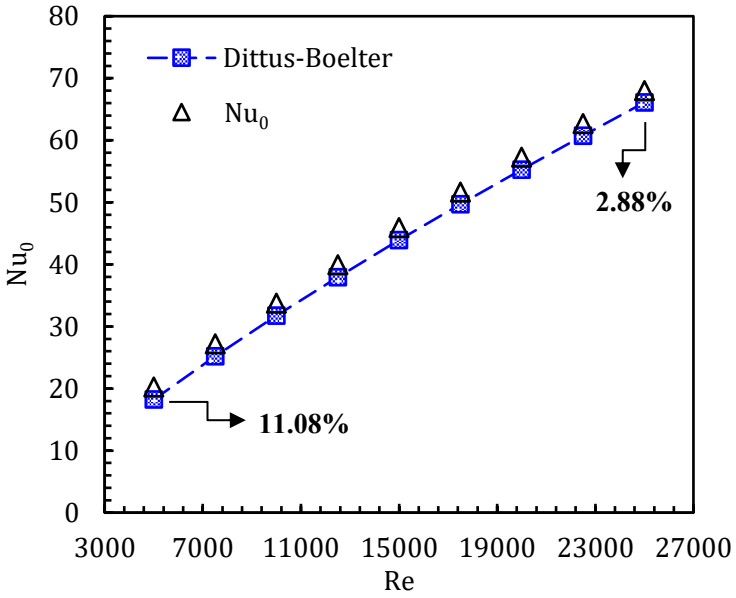

Figure 12. Comparison of Nu_0 results with the Dittus–Boelter correlation over the Reynolds number range Re=5000 to 25000

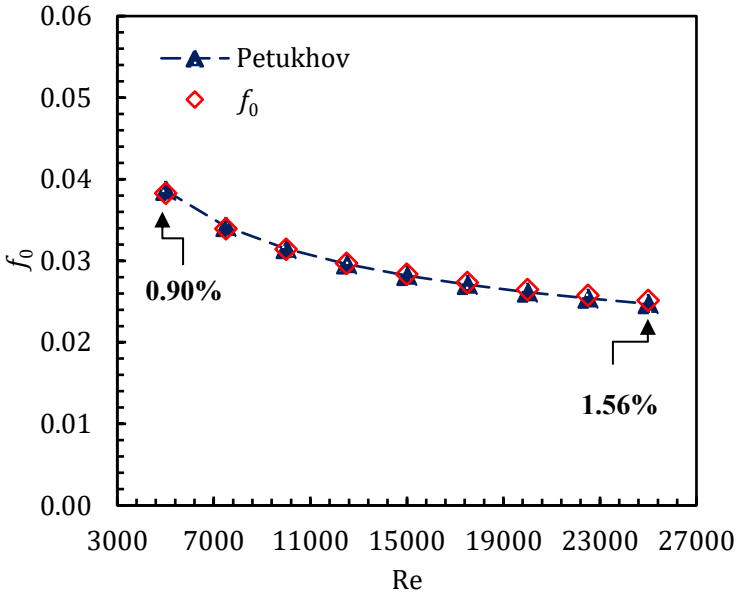

Figure 13. Comparison of f_0 with the Petukhov correlation over the Reynolds number range Re=5000 to 25000

Furthermore, the highest and the lowest deviation rates are attained to be 11.08% at $Re = 5000$ and 2.88% at $Re = 25000$ for Nu_0 as presented in Figure 12, while for f_0 the highest and the lowest deviation rates are calculated to be 1.56% at $Re = 25000$ and 0.90% at $Re = 5000$ as plotted in Figure 13. The values of free parameters applied in smooth pipe numerical studies within the range of $Re = 5000 - 25000$ are presented in Table 2 as stated below.

Table 2. Value of free parameters of *GEKO* turbulence model used in smooth pipe validation

Free Parameters	Value	Reynolds Number Range
C_{SEP}	1	5000-25000
C_{MIX}	$C_{MIXCOR} = 0.35sign(C_{SEP} - 1)\sqrt{(\lvert C_{SEP} - 1\rvert)}$	5000-25000
C_{NW}	-1.18-2	5000-25000
C_{NW-SUB}	1.7-2.5	5000-25000

3.3. The Comparative Parametric Evaluation of the CFPA and NCFPA Approaches

In this segment a parametric numerical examination is conducted to assess the influence of altering the number of *DWPs* ($N = 6, 5, 4,$ and 3), under both non-constant (*NCFPA*) and constant frontal projection area (*CFPA*) methodological approaches, on thermal-hydraulic characteristics within the range of $Re = 5000 - 25000$. *GEKO* turbulence model (with $C_{SEP} = 1.75$ and the

corresponding parameters of C_{MIXCOR}) is applied in the computational assessment of *DWPs* at $N = 3, 4, 5, 6$ and $3S$.

3.3.1. The NCFPA approach

In this part, a detailed numerical study is carried out to analyze the effect of varying the number of *DWPs* at $N = 6, 5, 4$, and 3 in a single row, without changing the geometric dimensions of the *DWPs*, on the thermal performance in the range of $Re = 5000 - 25000$.

3.3.1.1. Heat transfer

The variation of the Nusselt number of a smooth pipe as well as the pipe equipped with different numbers of *DWPs* and *Nu* number ratio, denoted as Nu/Nu_0, are shown in Figure 14 and Figure 15, respectively, in the Reynolds number range from 5000 to 25000.

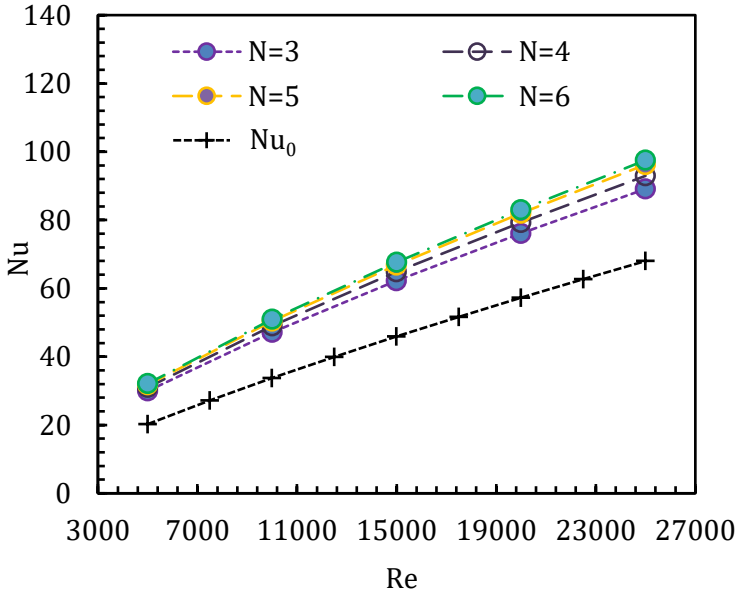

Figure 14. Variation of the Nusselt number for *DWP* configurations with N=3, 4, 5 and 6, including the smooth pipe baseline (Nu_0)

Similarly to what is observed in the case of the smooth pipe, the Nusselt numbers of $DWPs$ −inserted pipes demonstrate an increase in line with the rise in Reynolds numbers. This observation can be attributed to the increased ability of turbulent eddies to penetrate the thermal boundary layer at higher fluid velocities, thereby promoting fluid mixing at different temperatures and enhancing the Nusselt number. Furthermore, the $DWPs$, added pipes are detected to be exhibited higher Nusselt numbers within the range of $Re = 5000 - 25000$ compared to the

smooth pipe case. Additionally, the Nusselt number increases further with the rise in the number of $DWPs$. Thus, the highest Nu/Nu_0 ratios are obtained at $Re = 5000$ for $N = 6, 5, 4$ and 3 setups, respectively. This is because the longitudinal vortices induced by the *DWPs* prevent the development of the thermal boundary layer and act on the heated surface, thus increasing the Nusselt number at all Reynolds numbers.

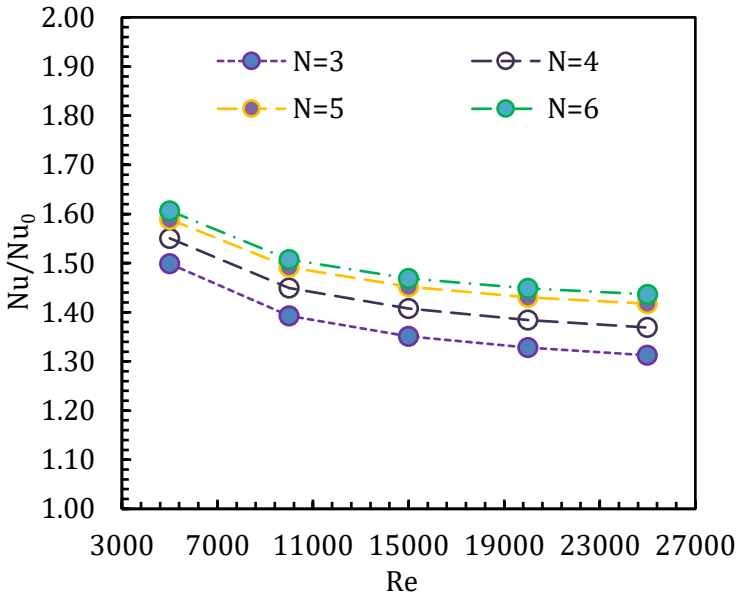

Figure 15. Variation of Nu/Nu_0 for *DWP* configurations with N=3, 4, 5 and 6

The streamlines passing in the vicinity of DWP are illustrated in Figure 16, with colors assigned in accordance with the respective local tangential Z-velocity magnitudes. As illustrated in Figure 16, each *DWP* generates two longitudinal vortices in *CFU* flow pattern on test region.

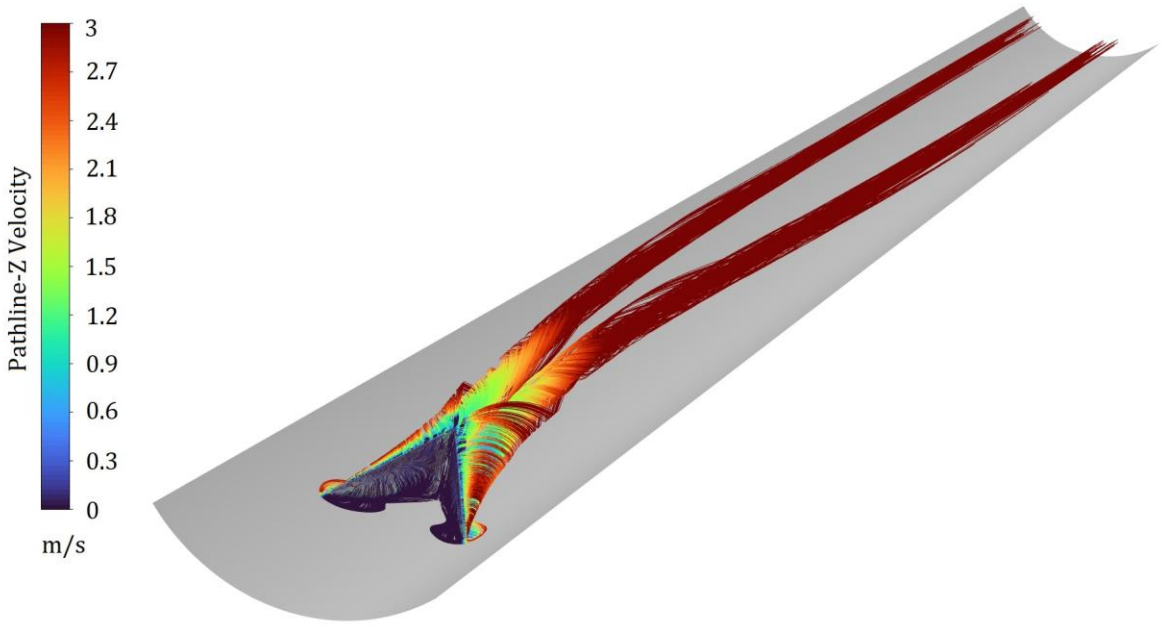

Figure 16. 3D representation of longitudinal vortices generated by *DWPs* with N=4 setup at Re=15000

Accordingly, when considering the streamline velocities, on a plane perpendicular to the main flow, at a distance of $P = 0.9\,m$ from the inlet, for $DWPs$ −equipped pipe at $N = 3, 4, 5$ and 6 setups, 6, 8, 10 and 12 main and secondary longitudinal vortices are detected to be initiated, respectively, as shown in Figure 17.

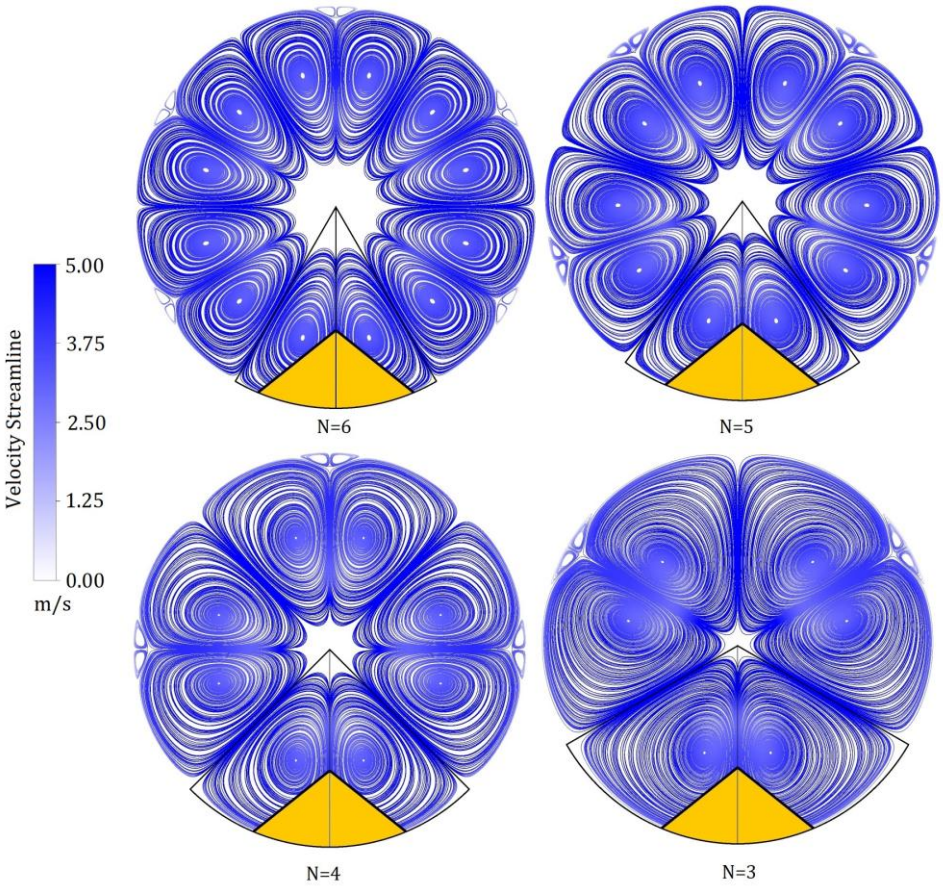

Figure 17. Time-averaged streamline patterns and axial (Z-direction) velocity contours for *DWPs* configurations (N = 3, 4, 5, and 6) at Re=15000 and P=0.9 m

In other words, increasing the number of $DWPs$ results in an increase in the presence of longitudinal vortices on the heated surface. Correspondingly, when examining the time-averaged contour maps of the temperature and local surface Nusselt number distributions, the lowest average temperature and highest average surface *Nu* numbers are obtained for $N = 6, 5, 4$ and 3 setups, respectively, as depicted in Figure 18. By examining the temperature contours on the heated surface (Figure 18), it is observed that the high-temperature regions (in red) decrease as the number of DWPs increases, leading to a noticeable drop in the area-weighted average temperature of heated surface, which can be taken as a sign of an increase in the Nusselt number as the number of $DWPs$ increases. Aside from the entrance region of test section, a distinct location within the test section exhibits a low temperature and a locally high Nusselt number are achieved at the trailing end of the $DWPs$. This is because the longitudinal vortices reach their peak strength at the trailing end and gradually weaken along the test section due to viscous forces. Thus, the area-weighted average temperature of heated surface is higher and the corresponding Nusselt number decreases close to the end of test region. As a conclusion, the numerical findings indicate that the

insertion of $DWPs$ into the pipe is thermally effective and thus, $DWPs$ −fitted pipes Nu/Nu_0 ratios are calculated to be ≥ 1 for $N = 3, 4, 5$, and 6 layouts within the $Re = 5000 - 25000$ range.

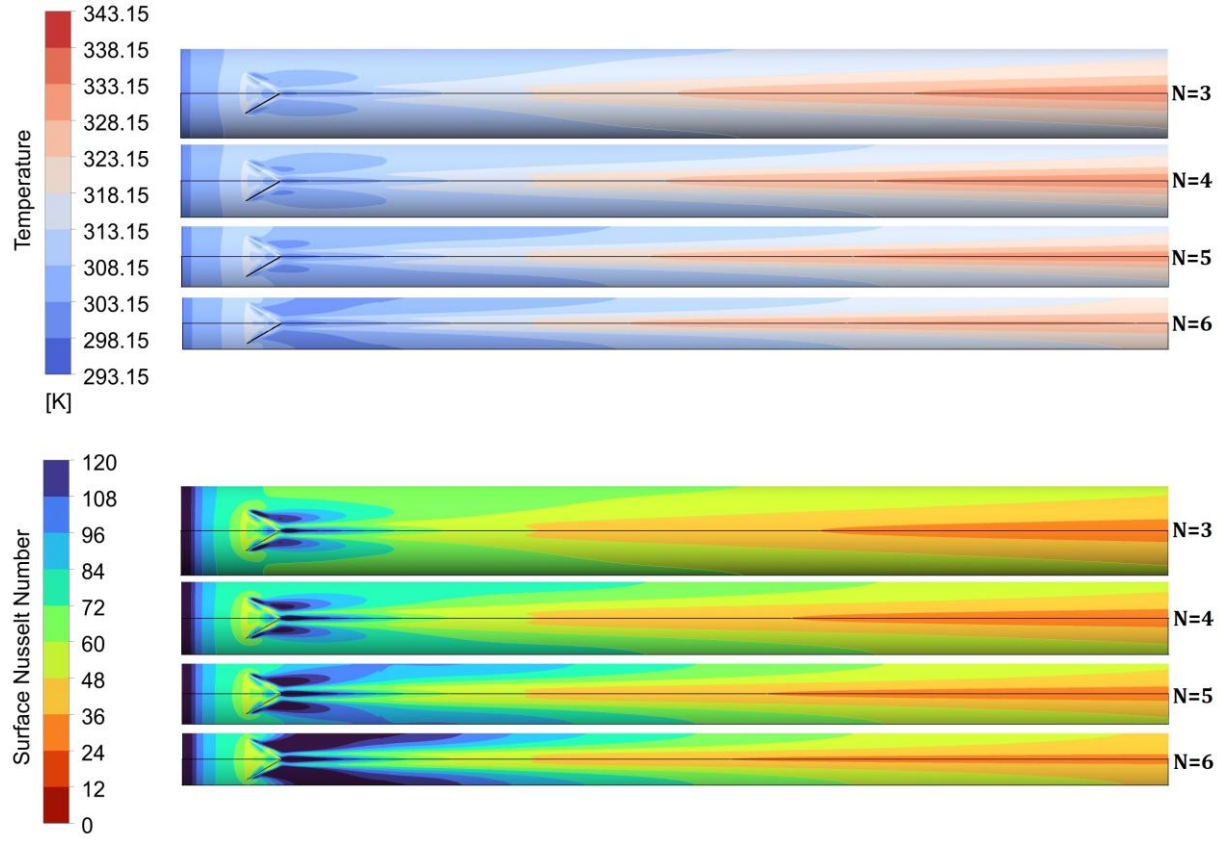

Figure 18. Time-averaged contour maps of temperature and local Nusselt number distributions for the *DWPs*-fitted pipe with N=3, 4, 5 and 6 arrangements at Re=15000

3.3.1.2. Friction factor

The variation of the Darcy friction factor, denoted as f, and the Darcy friction factor ratio, denoted as f/f0, of the $DWPs$ −equipped pipe with $N = 3, 4, 5$ and 6 configurations are plotted against the Reynolds number in the range of $Re = 5000 - 25000$ in Figure 19 and Figure 20, respectively. A significant increase in the Darcy friction factor compared to the smooth case is observed in cases where $DWPs$ are positioned at $N = 3, 4, 5$ and 6 setups as presented in Figure 19. Thus, f/f0 values are all calculated to be ≥ 1.00 for $N = 3, 4, 5$, and 6 layouts in the range of $Re = 5000 - 25000$. Factors such as the presence of longitudinal vortices as secondary flow, an enlarged contact surface area, intensified vortex interactions, and the increase in blockage ratio due to the presence of DWPs in the flow passage collectively contribute to the rise in the Darcy friction factor. Specifically, the blockage effect reduces the effective cross-sectional area available for the flow.

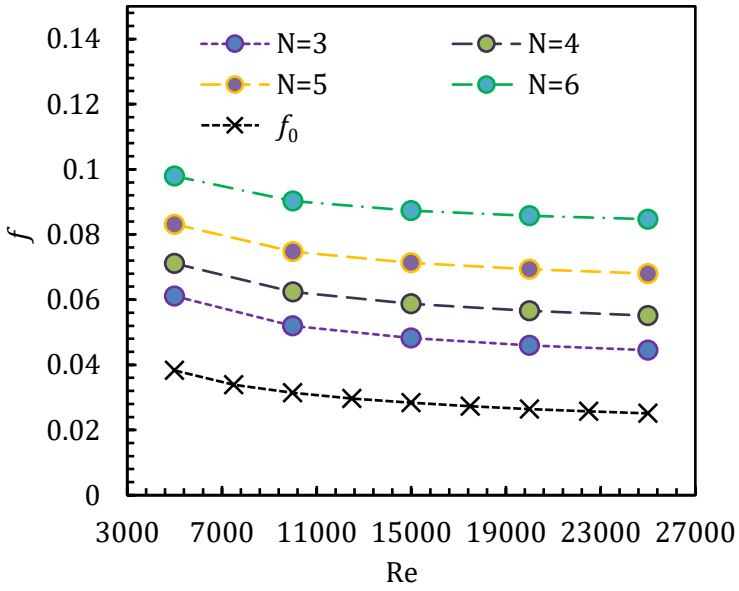

Figure 19. Variation of the Darcy friction factor for *DWP* configurations with N=3, 4, 5 and 6, including the smooth pipe baseline (f_0)

According to the principle of continuity, a decrease in flow area causes the local fluid velocity to increase within the constricted regions. Since the pressure drop is proportional to the square of velocity, this localized acceleration results in a disproportionately higher pressure loss, which directly translates into an increased friction factor.

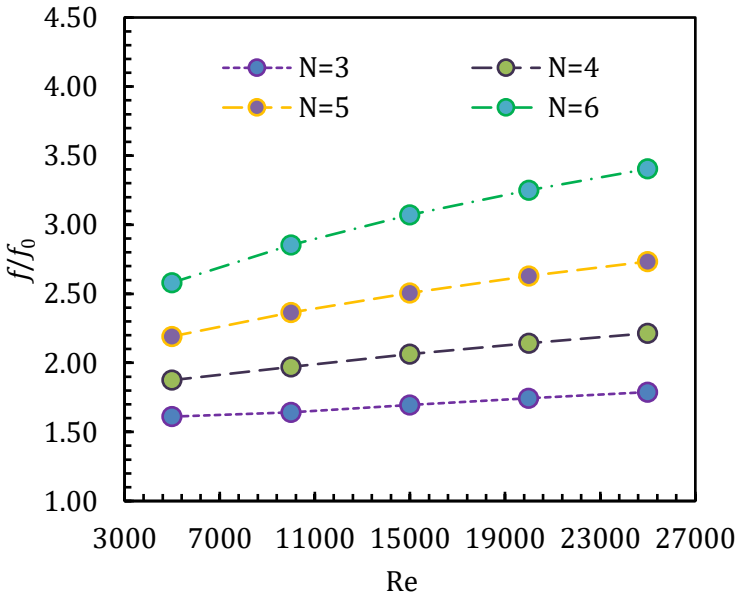

Figure 20. Variation of f/f_0 for *DWP* configurations with N=3, 4, 5 and 6

Moreover, the increase in the total wetted surface area enhances overall viscous dissipation, thereby contributing to a higher total frictional pressure loss. Additionally, the presence of winglets in the flow field forces the flow to change direction and mix, which increases the shear stress between adjacent fluid layers and further augments the total frictional resistance. In addition to that the successive addition of $DWPs$ in the test region, the effects of these factors are even amplified, leading to a non-linear, substantial increase in the overall flow resistance and the Darcy friction factor. Therefore, the highest Darcy friction factor and corresponding f/f0 ratios are obtained for $N = 6, 5, 4$ and 3 configurations, respectively.

3.3.1.3. Thermal enhancement factor

The variation of the Thermal Enhancement Factor (TEF) of $DWPs$ with $N = 3, 4, 5$ and 6 layouts, in relation to the Reynolds number is shown in Figure 21.

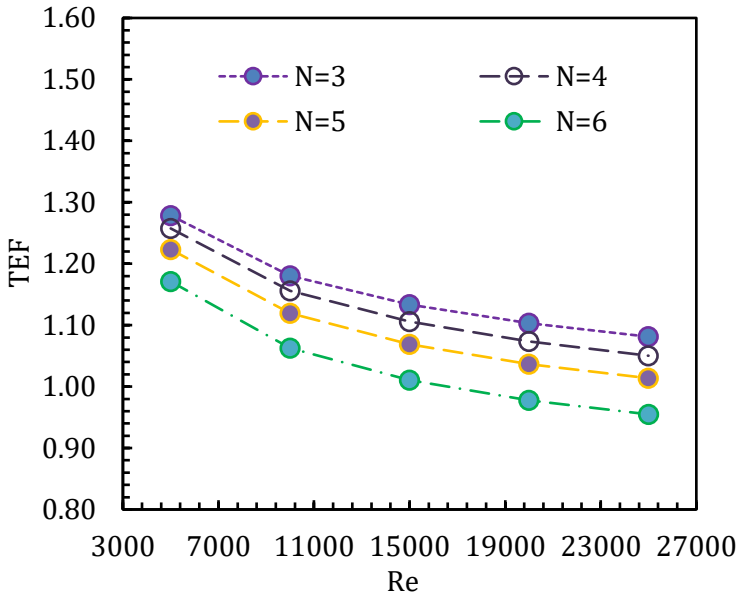

Figure 21. Comparison of TEF values for *DWP* arrangements with N=3, 4, 5 and 6

The *TEF* values for pipes fitted with different numbers of *DWPs* consistently decrease as the Reynolds number increases. At lower Reynolds number, the flow is less turbulent, and the longitudinal vortices generated by the *DWPs* have a dominant impact on breaking up the thermal boundary layer. As Reynolds number increases, the natural turbulence of the flow also increases, and the relative contribution of the *DWP*-induced vortices to the total mixing decreases, while the friction penalty rate continues to grow, leading to a lower *TEF*. The numerical investigation indicates that the *TEF* values for *DWPs* with $N = 3, 4, 5$ and 6 setups are calculated to be ≥ 1.00

even at Reynolds number as high as $Re = 25000$, with the exception of $N = 6$ configuration between $Re = 20000 - 25000$. This result clearly establishes that the insertion of *DWPs* at all *N* is effective in terms of *TEF* over a wide range of Reynolds numbers, resulting in the highest *TEF* values of 1.28, 1.26, 1.22 and 1.17 at $Re = 5000$ and 1.08, 1.05, 1.01 and ≈1.00 at $Re = 25000$ for $N = 3, 4, 5$ and 6 configurations, respectively.

3.3.2. The CFPA approach

This part of the numerical analysis evaluates the effect of different numbers of *DWPs*, arranged in a single row and configured to maintain a constant frontal projection area (*CFPA*), on the thermo-hydraulic behavior within the Reynolds number range of $5000 - 25000$. Furthermore, since the aspect ratio is a critical parameter influencing *VG* performance, as highlighted in the preceding section, the aspect ratios of the *DWPs* in the $N = 6$ and $N = 3S$ configurations are kept constant.

3.3.2.1. Heat transfer

A comparison of the Nusselt number and the corresponding Nu/Nu_0 variations over the Reynolds number range of $5000 - 25000$ for the *DWPs* configurations with $N = 6$ and $N = 3S$, positioned in a single row within the test section while maintaining a constant total frontal projection area, is presented in Figure 22 and Figure 23, respectively. The calculated Nusselt number in both cases of *DWPs* is much higher than the smooth pipe Nusselt number as plotted in Figure 22.

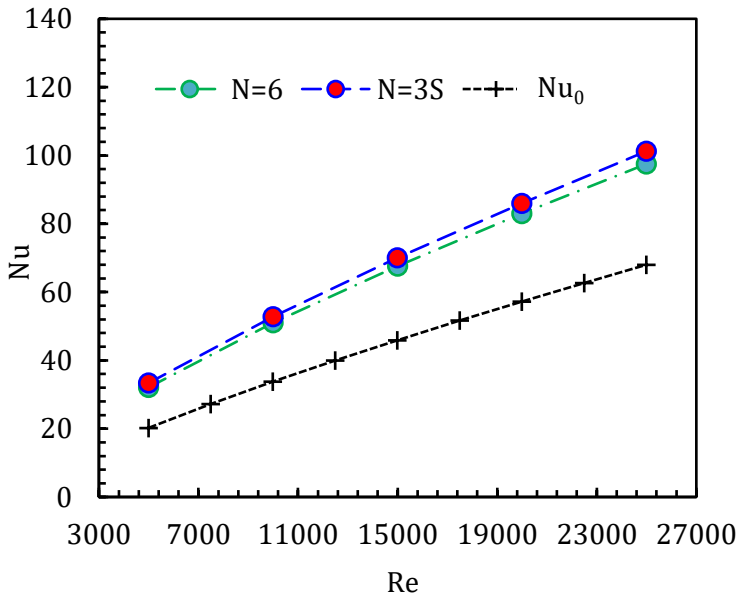

Figure 22. Variation of the Nusselt number for *DWP* configurations with N=3S and 6, including the smooth pipe baseline (Nu_0)

Heat transfer through the pipe wall is governed by the thermal boundary layer, a thin layer of fluid adjacent to the heated wall where temperature changes rapidly. In a smooth pipe, heat transfer takes place primarily through this relatively stationary layer by slow conduction. The high resistance of this layer limits the overall heat transfer rate. The powerful longitudinal vortices induced by *DWPs*, leads the cooler fluid from the core of the pipe directly towards the heated pipe wall and simultaneously lift the heated fluid from the heated surface back into the core flow. This continuous cross-stream mixing or swirling motion of fluid effectively thins, disrupts, and re-growth the thermal boundary layer along the test section of pipe. By constantly replacing the hot fluid near the heated wall with cooler core fluid, the *DWPs* maintain a steeper temperature gradient at the heated wall, leading to a higher local heat flux and consequently a significant enhancement in the convective heat transfer coefficient (h) and the overall Nusselt number. Moreover, the *DWPs* enhance heat transfer not only by disturbing the thermal boundary layer but also by substituting the slow molecular diffusion near the heated wall with the much more efficient eddy diffusion mechanism induced by elevated turbulence intensity and the strong, organized mixing generated by the longitudinal vortices. This clearly demonstrates that the inclusion of *DWPs* in both $N = 6$ and $N = 3S$ configurations has a pronounced impact on improving the overall thermal performance.

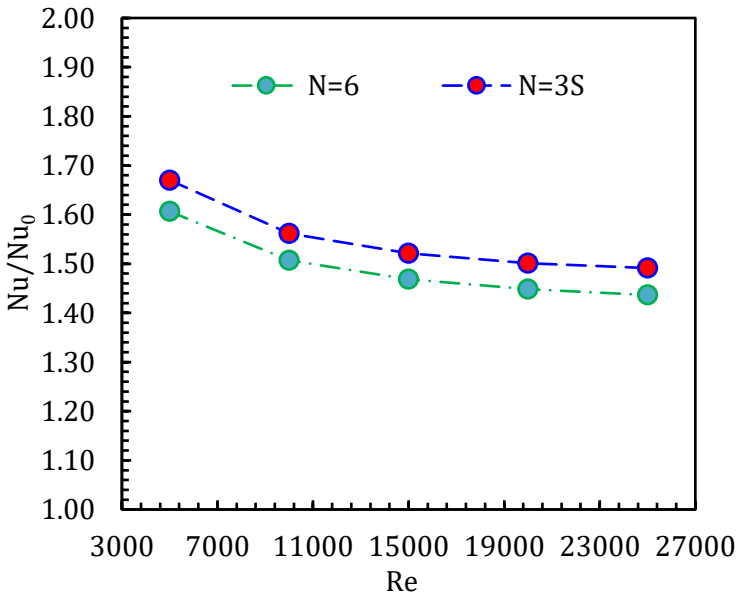

Figure 23. Variation of Nu/Nu_0 for *DWP* configurations with N=3S and 6

Essentially, both cases of $N = 6$ and $N = 3S$ arrangements provide higher Nusselt number in comparison to the case of smooth pipe across all Reynolds number, resulting in $Nu/Nu_0 \geq 1$.

Furthermore, a comparison of $N = 6$ and $N = 3S$ configurations of *DWPs* reveals that the $N = 3S$ setup exhibits higher Nusselt number and Nu/Nu_0 ratios relative to the $N = 6$ layout. Based on the attained numerical data, even though, increased number of longitudinal vortices results in greater Nu number in previous section, the numerical data in this section present opposite results. In particular, despite the presence of 12 longitudinal vortices on test region for the case of $N = 6$ setup, there are only 6 longitudinal vortices are present for $N = 3S$ arrangement. In order to provide a visual illustration of this situation, a comparative presentation of the time-averaged streamline velocity distribution in the plane perpendicular to the $Z-$axis and the vorticity$-Z$ contour map in the plane perpendicular to the main flow at $P = 0.9$ m is provided in Figure 24.

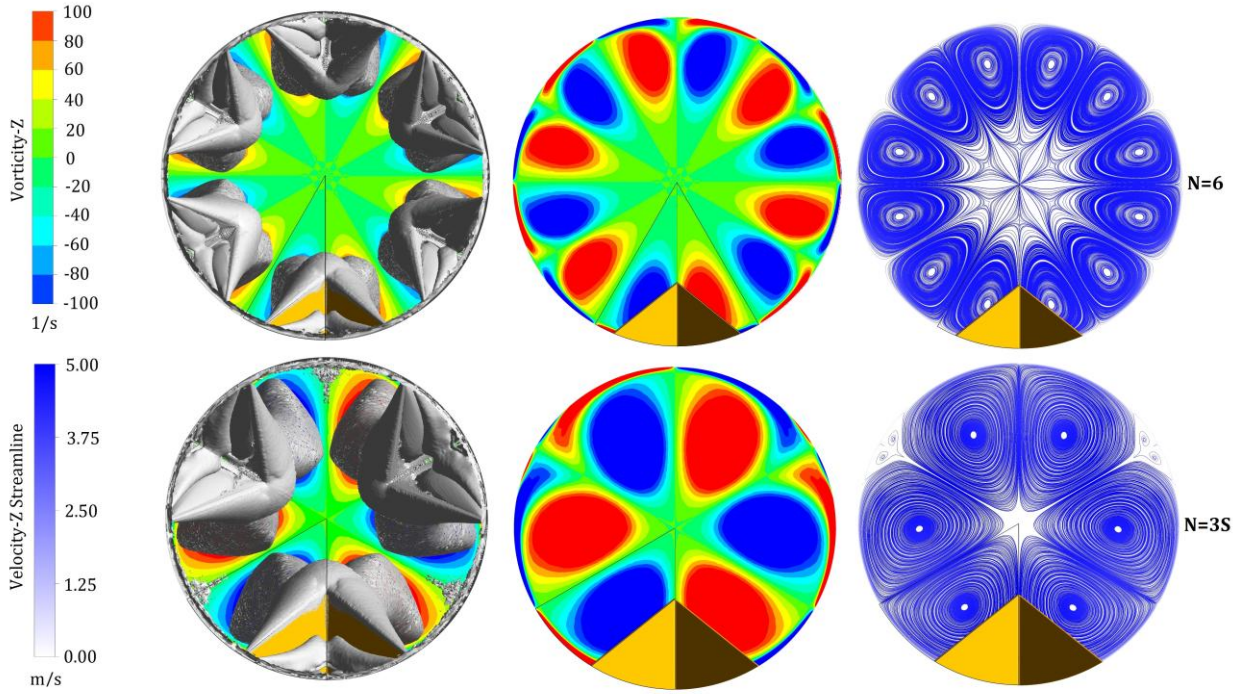

Figure 24. Time-averaged streamline velocity distribution in the plane perpendicular to the Z-axis, vorticity in the Z-direction contour map, and vortex structures identified using the Q-criterion (level set to 0.0003) for *DWPs* with N=6 and N=3S at Re=15000

Based on the data presented in Figure 24, *DWPs* with $N = 3S$ setup produces noticeably stronger and thus effective on a larger scale vortices than $N = 6$ configuration, which indicate strong rotational effects or vortices in the plane perpendicular to the flow direction. Moreover, the observations indicate that although the $N = 6$ configuration introduces a greater number of longitudinal vortices, these vortices are relatively weaker and remain confined to the near-wall region. In contrast, the $N = 3S$ configuration, despite having fewer winglets, generates stronger

vortices that penetrate deeper into the core flow. These vortices enhance momentum exchange and heat transport throughout the entire cross-section, resulting in a more effective overall thermal enhancement, leading to the Nu/Nu_0 ratios of the $N = 3S$ case are calculated to be higher than the $N = 6$ arrangement. Additionally, the comparative presentation of contour maps of temperature for $N = 6$ and $N = 3S$ layouts are also provided on planes perpendicular to the main flow at 8 distances from the inlet along the test region Figure 25-a), with the objective of further visually revealing and clarifying the phenomena stated above. The dead zones (high temperature regions in Figure 25-b) that is, the spaces between two longitudinal vortices that are unaffected by the vortices, are considerably reduced in the case of $N = 3S$ compared to the case of $N = 6$. Thus, the incorporation of *DWPs* with $N = 3S$ setup results in the attainment of elevated Nusselt number and correspondingly elevated Nu/Nu_0 ratios when compared to $N = 6$ arrangement within the range of $Re = 5000 - 25000$.

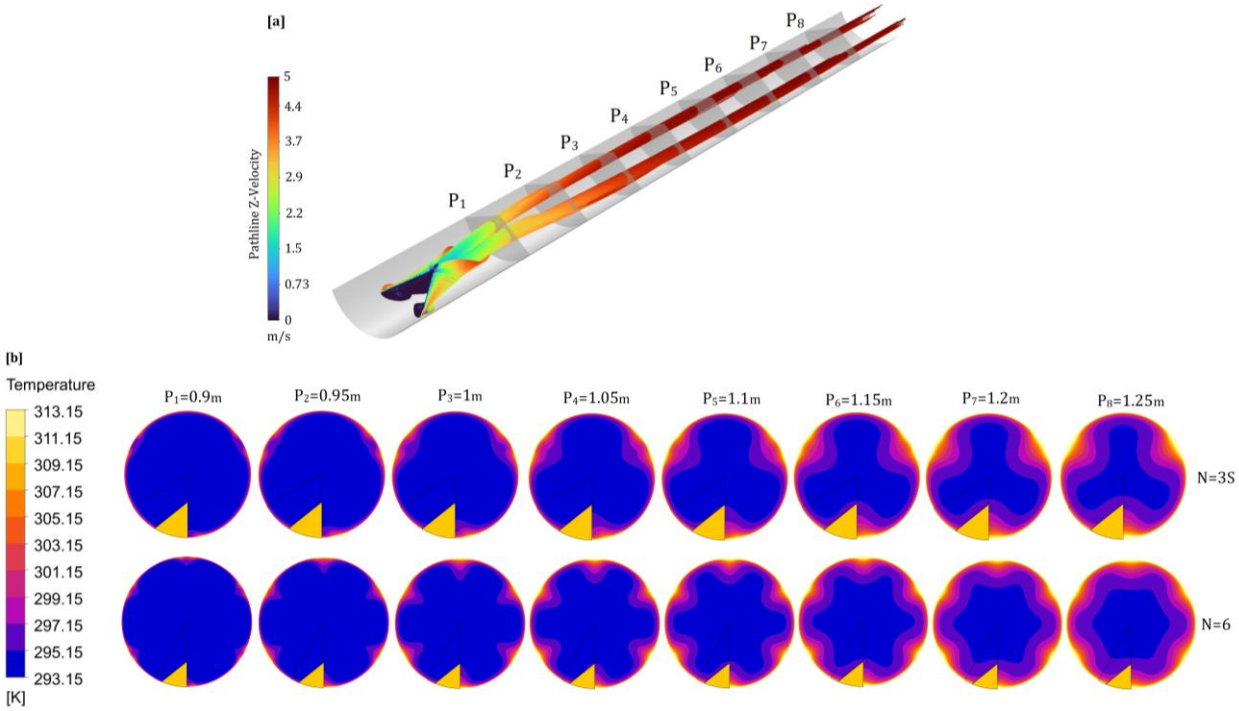

Figure 25. Time-averaged (a) pathlines colored by axial velocity (Z-direction) and (b) temperature contour maps for *DWPs* with N=3S and N=6 layouts at Re=15000

3.3.2.2. Friction factor

The effects of varying the number of *DWPs*, including $N = 3S$ and $N = 6$ configurations under *CFPA* approach, on the pressure loss characteristics are plotted and compared with the data for the smooth pipe case within $Re = 5000 - 25000$ range, as presented in Figure 26. In a manner

analogous to that is observed in smooth pipe case, the Darcy friction factors, f, exhibit a declining trend with an increase in the Reynolds number, while f/f_0 ratios demonstrate an upward trend in both cases of $N = 3S$ and $N = 6$. Thus, the lowest value of f/f_0 and the highest Darcy friction factor are attained at $Re = 5000$. Furthermore, the resulting numerical data indicate that insertion of *DWPs* in both $N = 3S$ and $N = 6$ configurations result in higher f values in comparison to the smooth pipe case, leading to f/f_0 ratios that are significantly greater than >1.00 (Figure 27).

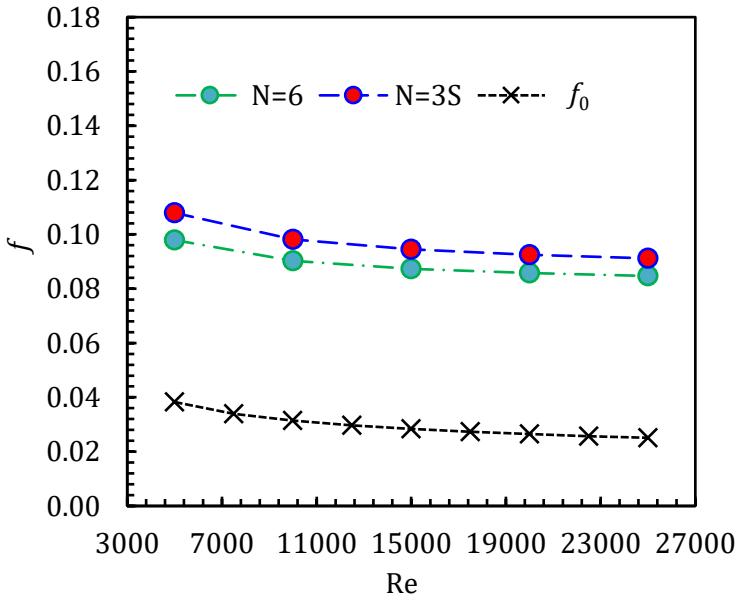

Figure 26. Variation of the Darcy friction factor for *DWP* configurations with N=3S and 6, including the smooth pipe baseline (f_0)

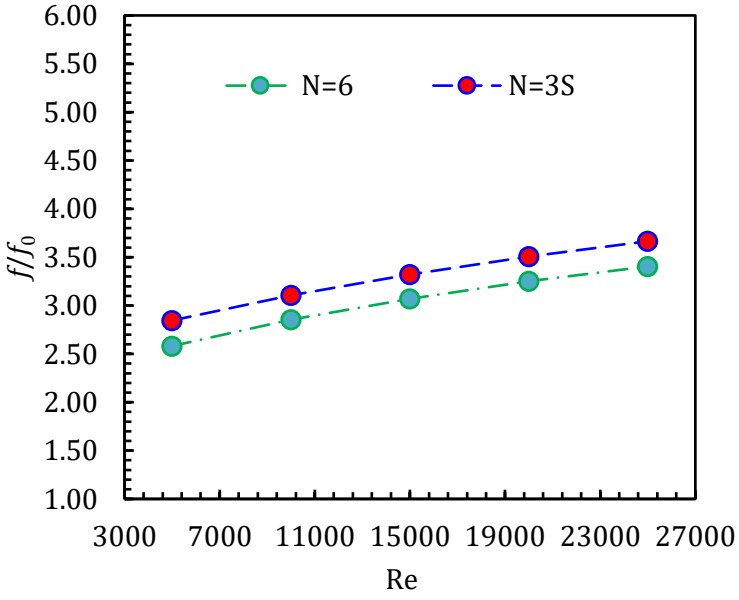

Figure 27. Variation of f/f_0 for *DWP* configurations with N=3S and 6

The notable rise in Darcy friction factors are attributed mainly to the size of the frontal projection area of *VGs* within the flow field along with the previously indicated factors. The observed increase in the ratio of f/f_0 with rising Reynolds number is primarily attributed to the disproportionate growth of form drag induced by the *DWPs* in both cases. As the fluid velocity increases with Reynolds number, flow separation and wake formation around the *DWPs* cause the associated pressure losses to rise at an accelerating, disproportionate rate, whereas the frictional resistance in the smooth pipe decreases slightly. Consequently, this non-linear increase of total pressure drop, driven by stronger wake-induced pressure losses and enhanced vortex-induced energy dissipation, leads to a pronounced increase in the f/f_0 ratio as the flow becomes faster and more turbulent. Furthermore, the pressure loss differential between the leading and trailing edges of the *VGs* serves as a strong indicator of the longitudinal vortex strength within the test region. In this context, the $N = 3S$ arrangement not achieves higher Nusselt numbers but also exhibits an elevated Darcy friction factor and f/f_0 values compared to the $N = 6$ configuration across all Reynolds numbers, reflecting the influence of stronger, more deeply penetrating vortices on both heat transfer and flow resistance. As noted previously, to maintain a constant total frontal projection area across both *DWP* configurations, the geometry of the *DWPs* in the $N = 3S$ layout is scaled up by approximately $S = 1.46{:}\,1$. Although the frontal projection areas are identical, this geometric scaling markedly influences the observed differences between $N = 3S$ and $N = 6$ configurations in terms of flow structure. To illustrate this effect, Figure 28 presents a comparison of the vortical structures identified by the Q −criterion and the corresponding velocity vector distributions on the symmetry plane for each configuration at $Re = 15000$.

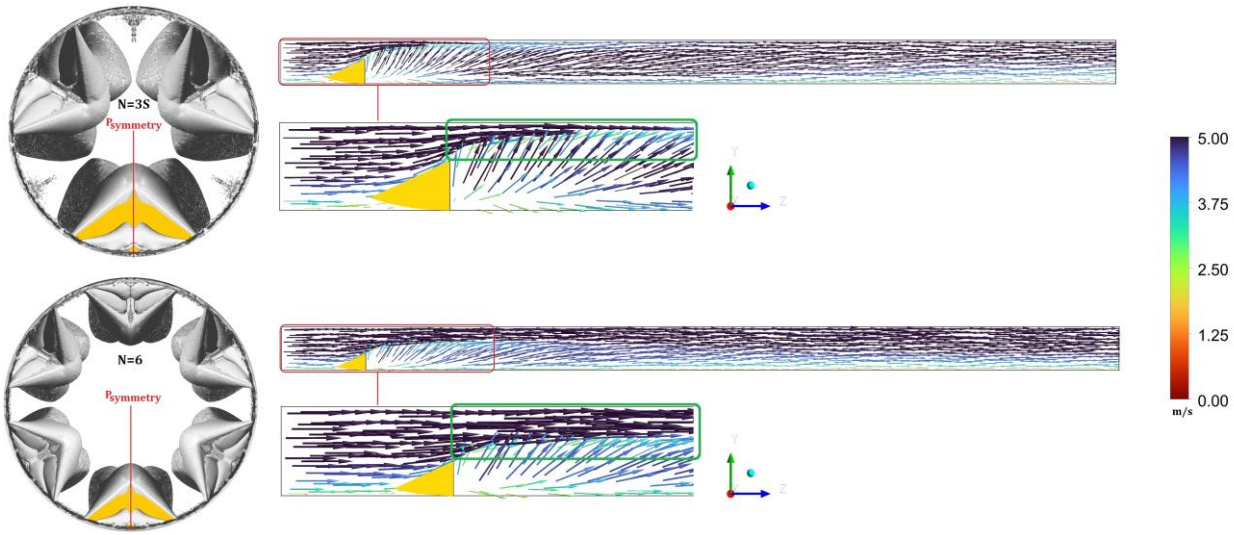

Figure 28. Vortical structure using the Q-criterion (level set to 3×10^{-4}) and the velocity vector distribution on $P_{symmetry}$ for *DWPs* with N=3S and N=6 layouts

In the $N = 3S$ configuration, the vortices are more pronounced and exert a greater influence over a larger cross-sectional area within the pipe flow. This forces the main flow through a narrower region, despite having only half the number of vortices compared to the $N = 6$ configuration. This effect is notably evident in the central region of flow section of pipe, which is substantially narrower in the $N = 3S$ case than in the $N = 6$ case. This phenomenon can be readily observed in the green boxed area of the time-averaged velocity vector distribution on $P_{symmetry}$. Consequently, despite the fact that the frontal projection areas of both $N = 3S$ and $N = 6$ configurations are equal, the $N = 3S$ configuration exhibits higher Darcy friction factors and corresponding f/f_0 ratios in the Reynolds number range of $5000 - 25000$ due to the cited factors.

3.3.2.3. Thermal enhancement factor

The change in *TEF* values of both cases of *DWP* configurations, including $N = 3S$ and $N = 6$ layouts, are plotted against to Reynolds number in Figure 29. Despite the considerable increase in Darcy friction factor for the case of *DWP* with $N = 3S$ setup, an increase in heat transfer performance is even higher in comparison to the case of *DWP* with $N = 6$ configuration. Thus, in addition to Nu/Nu_0 and f/f_0 ratios, the $N = 3S$ configuration of the *DWP* also yields higher values of *TEF* within $Re = 5000 - 25000$ range. This leads to the highest and lowest *TEF* values being achieved as 1.18 and 1.17 at $Re = 5000$ and ≈1.00 for both cases at $Re = 25000$ for *DWPs* with $N = 3S$ and $N = 6$ arrangements, respectively.

To summarize all the numerical findings in terms of *TEF*, the rates of increase in *TEF* are 9.18% and 0.63% at $Re = 5000$ and 13.23% and 1.30% at $Re = 25000$ for *NCFPA* ($N = 3$ case) and *CFPA* ($N = 3S$ *case*) approaches, respectively, compared to the reference case of *DWPs* with $N = 6$ configuration (Figure 29). The computational results lead to the conclusion that the change in the number of *DWPs*, considering *NCFPA* approach has a much more pronounced effect on the *TEF* compared to the *CFPA* approach.

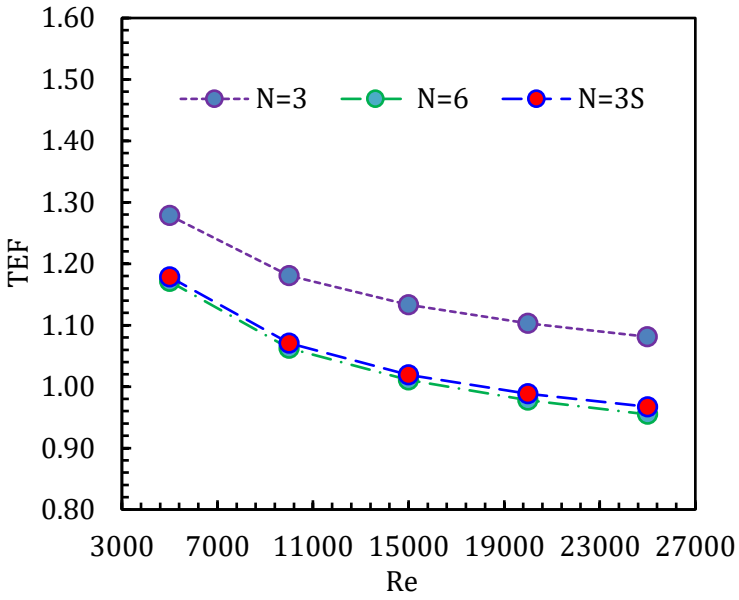

Figure 29. Variation of TEF for *DWP* configurations with N=3S, 3 and 6

4. CONCLUSION

This section presents an overview of the key findings from the detailed numerical assessment of the *NCFPA* and *CFPA* approaches, focusing on both heat transfer and friction factor characteristics, and highlights the capability of the *GEKO* turbulence model in accurately predicting turbulent flow behavior across different applications. The summary of the computational results are:

1. The validation of the experimental data for *DWs* with $\alpha = 40°$, $s = 10\ mm$ and $h = 10\ mm$ shows that, the utilization of $C_{SEP} = 1.75$ and the corresponding C_{MIXCOR}, the calculated mean average deviations for $Nu_{Exp.}$, $f_{Exp.}$ and TEF_{Exp} are 4.80%, 1.85% and 4.99%, respectively.
2. The performance assessment of *GEKO* turbulence model also encompasses the validation of a smooth pipe, resulting in mean absolute deviation rates of 5.42% for Nu_0 and 0.85% for f_0 in comparison with the Dittus-Boelter and Petukhov correlation equations. The determined values of free parameters of *GEKO* turbulence model are in the range of $C_{NW} = -1.18 - 2, C_{NW-SUB} = 1.7 - 2.5,$ $C_{SEP} = 1$ and the corresponding C_{MIXCOR}.
3. Under *NCFPA* approach, the *DWPs*−fitted pipe with $N = 3$ setup demonstrates a significantly lower Darcy friction factor in comparison to the case of $N = 4, 5$ and 6 configurations. Accordingly, for $N = 4, 5,$ and 6, the percentage increases

in f/f_0 relative to $N = 3$ are calculated to be 16.40% and 23.83%; 36.07% and 52.86%; and 60.25% and 90.36% at $Re = 5000$ and $Re = 25000$, respectively. This demonstrates that, among the configurations considered, $N = 3$ offers the lowest pressure losses throughout the test section.

4. Under the *CFPA* constraint, scaling the *DWP* geometry markedly influences both the heat transfer and flow characteristics. Specifically, the *DWP* with *N=3S* setup generates the strongest vortices, which constrict the main flow through a narrower region, leading to highest both f/f_0 and Nu/Nu_0 among other configurations investigated.
5. Under the *CFPA* approach, the $N = 3S$ configuration exhibits percentage increases relative to $N = 6$ of 10.25% and 7.65% for f/f_0, and 3.96% and 3.82% for Nu/Nu_0 at $Re = 5000$ and $Re = 25000$, respectively.
6. In the *CFPA* approach, although friction increases notably for $N = 3S$, the improvement in heat transfer surpasses the associated frictional losses, resulting in a *TEF* of 1.18 at $Re = 5000$ and approximately 1.00 at $Re = 25000$. Overall, the *NCFPA* approach exhibits a more pronounced *TEF* enhancement compared to *CFPA*, with the highest *TEF* values achieved using *DWPs* in the $N = 3$ configuration. Specifically, *TEF* reaches 1.28 at $Re = 5000$ and 1.08 at $Re = 25000$.

NOMENCLATURE

Symbol	
f	Darcy friction factor,-
h	The heigt of DWP, mm
Nu	The Nusselt number,-
l	The base length of the DWP, mm
Abbreviation	
CFPA	Constant Frontal Projected Area
DW	Delta Winglet
DWP	Delta Winglet Pair
GEKO	GEneralized K-Omega Turbulence Model
N	Number (of DWPs positioned on the inner pipe wall)
NCFPA	Non-Constant Frontal Projected Area
TEF	Thermal Enhancement Factor
RANS	Reynolds Averaged Navier Stokes

S	Scaling (=1.46:1)
VG	Vortex Generator

ACKNOWLEDGMENT

The authors would like to acknowledge that part of the numerical validation data presented in this work is based on the master's thesis titled "*Numerical Investigation of the Thermal Performance of Innovative Vortex Generator Designs Placed on the Heated Surface in a Pipe with the GEKO Turbulence Model*," conducted by Necip Hazer at Yozgat Bozok University.

DECLARATION OF ETHICAL STANDARDS

The authors of the paper submitted declare that nothing which is necessary for achieving the paper requires ethical committee and/or legal-special permissions.

CONFLICT OF INTEREST

There is no conflict of interest in this study.

CONTRIBUTION OF THE AUTHORS

Hüseyin Zahit Demirağ: Conceptualization, Methodology, Software, Formal analysis, Investigation, Writing - original draft.

Atila Abir İğci: Conceptualization, Methodology, Software, Formal analysis, Writing - review & editing.

Necip Hazer: Validation, Data curation, Investigation.

REFERENCES

[1] Sheikholeslami M, Gorji-Bandpy M, Ganji DD. Review of heat transfer enhancement methods: focus on passive methods using swirl flow devices. Renew Sustain Energy Rev 2015; 49: 444-469.

[2] Bergles AE. ExHFT for fourth generation heat transfer technology. Exp Therm Fluid Sci 2002; 26: 335-344.

[3] Liu S, Sakr M. A comprehensive review on passive heat transfer enhancements in pipe exchangers. Renew Sustain Energy Rev 2013; 19: 64-81.

[4] Bhattacharyya S, Vishwakarma DK, Srinivasan A, Soni MK, Goel V, Sharifpur M, et al. Thermal performance enhancement in heat exchangers using active and passive techniques: a detailed review. J Therm Anal Calorim 2022; 147: 9229-9281.
[5] Min C, Qi C, Kong X, Dong J. Experimental study of rectangular channel with modified rectangular longitudinal vortex generators. Int J Heat Mass Transf 2010; 53: 3023-3029.
[6] Xu Z, Han Z, Wang J, Liu Z. The characteristics of heat transfer and flow resistance in a rectangular channel with vortex generators. Int J Heat Mass Transf 2018; 116: 61-72.
[7] Fiebig M. Vortices, generators and heat transfer. Chem Eng Res Des 1998; 76: 108-123.
[8] Tian LT, He YL, Lei YG, Tao WQ. Numerical study of fluid flow and heat transfer in a flat-plate channel with longitudinal vortex generators by applying field synergy principle analysis. Int Commun Heat Mass Transf 2009; 36: 111-120.
[9] Jacobi AM, Shah RK. Heat transfer surface enhancement through the use of longitudinal vortices: a review of recent progress. Exp Therm Fluid Sci 1995; 11: 295-309.
[10] Tang LH, Chu WX, Ahmed N, Zeng M. A new configuration of winglet longitudinal vortex generator to enhance heat transfer in a rectangular channel. Appl Therm Eng 2016; 104: 74-84.
[11] Fiebig M. Vortices and heat transfer. ZAMM Zeitschrift Fur Angew Math Und Mech 1997; 77: 3-18.
[12] Sohankar A. Heat transfer augmentation in a rectangular channel with a vee-shaped vortex generator. Int J Heat Fluid Flow 2007; 28: 306-317.
[13] Wang J, Fu T, Zeng L, Lien FS, Deng X, Zhang F. Heat transfer performance of internal flow by inserting punched and non-punched vortex generators. Int J Therm Sci 2023; 186.
[14] Wang J, Fu T, Zeng L, Lien FS, Chen G. Thermal-hydraulic performance in a tube with punched delta winglets inserts in turbulent flow. Int J Therm Sci 2022; 172.
[15] Liu HL, Li H, He YL, Chen ZT. Heat transfer and flow characteristics in a circular tube fitted with rectangular winglet vortex generators. Int J Heat Mass Transf 2018; 126: 989-1006.
[16] Wu X, Fu T, Wang J, Zeng L, Zhang F. A comparative study of fluid flow and heat transfer in the tube with multi-V-winglets vortex generators. Appl Therm Eng 2024; 236.
[17] Sun Z, Zhang K, Li W, Chen Q, Zheng N. Investigations of the turbulent thermal-hydraulic performance in circular heat exchanger tubes with multiple rectangular winglet vortex generators. Appl Therm Eng 2020; 168.
[18] Sun Z, Chen Q, Zheng N. Experimental and numerical studies of intensified turbulent heat transfer in round pipes with curved wing vortex generators. Int J Heat Mass Transf 2021; 180.

[19] Xu Y, Islam MD, Kharoua N. Numerical study of winglets vortex generator effects on thermal performance in a circular pipe. Int J Therm Sci 2017; 112: 304-317.
[20] Liang G, Islam MD, Kharoua N, Simmons R. Numerical study of heat transfer and flow behavior in a circular tube fitted with varying arrays of winglet vortex generators. Int J Therm Sci 2018; 134: 54-65.
[21] Promvonge P, Promthaisong P, Skullong S. Experimental and numerical heat transfer study of turbulent tube flow through discrete V-winglets. Int J Heat Mass Transf 2020; 151.
[22] Zhang K, Sun Z, Zheng N, Chen Q. Effects of the configuration of winglet vortex generators on turbulent heat transfer enhancement in circular tubes. Int J Heat Mass Transf 2020; 157.
[23] M MS, Fernandes DV. Numerical investigation of heat transfer and friction factor characteristics of circular tube fitted with an array of semi-elliptical vortex generator inserts. Cogent Eng 2021; 8.
[24] Min C, Li H, Gao X, Wang K, Xie L. Numerical investigation of convective heat transfer enhancement by a combination of vortex generator and in-tube inserts. Int Commun Heat Mass Transf 2021; 127: 105490.
[25] Jayranaiwachira N, Promvonge P, Promthaisong P, Nakhchi ME, Skullong S. Heat transfer analysis in a tube contained with louver-punched triangular baffles. Results Eng 2024; 22: 102276.
[26] Habchi C, Russeil S, Bougeard D, Harion JL, Lemenand T, Della Valle D, et al. Enhancing heat transfer in vortex generator-type multifunctional heat exchangers. Appl Therm Eng 2012; 38: 14-25.
[27] Ke Z, Chen CL, Li K, Wang S, Chen CH. Vortex dynamics and heat transfer of longitudinal vortex generators in a rectangular channel. Int J Heat Mass Transf 2019; 132: 871-885.
[28] Joardar A, Jacobi AM. Impact of leading edge delta-wing vortex generators on the thermal performance of a flat tube, louvered-fin compact heat exchanger. Int J Heat Mass Transf 2005; 48: 1480-1493.
[29] Incropera FP, DeWitt DP. Fundamentals of heat and mass transfer. 5th ed. New York: John Wiley & Sons; 2002.
[30] Zhai C, Islam MD, Simmons R, Barsoum I. Heat transfer augmentation in a circular tube with delta winglet vortex generator pairs. Int J Therm Sci 2019; 140: 480-490.
[31] Fiebig M. Embedded vortices in internal flow: heat transfer and pressure loss enhancement. Int J Heat Fluid Flow 1995; 16: 376-388.
[32] Kareem ZS, Mohd Jaafar MN, Lazim TM, Abdullah S, Abdulwahid AF. Passive heat transfer enhancement review in corrugation. Exp Therm Fluid Sci 2015; 68: 22-38.

[33] Versteeg HK, Malalasekera W. An introduction to computational fluid dynamics: The finite volume method. 2nd ed. Pearson Education; 2007.

[34] Menter FR, Lechner R, Matyushenko A. Best practice: Generalized k-ω two-equation turbulence model in ANSYS CFD (GEKO). ANSYS Inc; 2019.

[35] Hazer N. Numerical investigation of the thermal performance of innovative vortex generator designs placed on the heated surface in a pipe with the GEKO turbulence model [Master's thesis]. Yozgat Bozok University; 2025.

[36] Ali S, Habchi C, Zaytoun H, Khaled M, Dbouk T. Surrogate-based optimization of the attack and inclination angles of a delta winglet pair vortex generator in turbulent channel flow. Int J Thermofluids 2023; 20: 100473.

[37] Zheng N, Zhang K, Chen Q, Sun Z. Novel self-join winglet vortex generators for enhanced heat transfer of turbulent airflow in round tubes. Int Commun Heat Mass Transf 2022; 130: 105806.

[38] Dittus FW, Boelter LMK. Heat transfer in automobile radiators of the tubular type. Int Commun Heat Mass Transf 1985; 12: 3-22.

[39] Petukhov BS. Heat transfer and friction in turbulent pipe flow with variable physical properties. Adv Heat Transf 1970; 6: 503-564.